Asymmetric dark matter with a spontaneously broken $U(1)'$: Self-interaction and gravitational waves

Zien Chen, Kairui Ye, and Mengchao Zhang*

Department of Physics and Siyuan Laboratory, Jinan University, Guangzhou 510632, People's Republic of China

(Received 25 March 2023; accepted 5 May 2023; published 18 May 2023)

Motivated by the collisionless cold dark matter small scale structure problem, we propose an asymmetric dark matter model with the dark sector charged under a dark $U(1)'$. The mediator between dark matter particles is the dark gauge boson, which obtains its mass through the spontaneous breaking of $U(1)'$. This model easily avoids the strong limits from cosmic microwave background (CMB) observation, and has a large parameter space to be consistent with small scale structure data. We focus on a special scenario where portals between the dark sector and visible sector are too weak to be detected by traditional methods. We find that this scenario can increase the effective number of neutrinos ($N_{\rm eff}$). In addition, the spontaneous $U(1)'$ symmetry breaking process can generate stochastic gravitational waves with peak frequency around 10^{-6}–10^{-7} Hz.

DOI: 10.1103/PhysRevD.107.095027

I. INTRODUCTION

There has been plenty of evidence for the existence of dark matter (DM) [1,2], but the nature of DM still remains to be revealed. Collisionless cold DM is consistent with the large scale structure of the Universe [3,4]. However, N-body simulations of collisionless cold DM show some discrepancies between predictions and observations on the scale smaller than $\mathcal{O}$(Mpc). Those discrepancies include the core-cusp problem [5–7], diversity problem [8], missing satellites problem [9,10], and too-big-to-fail (TBTF) problem [11,12]. Including baryon effects in the simulation helps to alleviate some tension [13,14], but it is still unclear whether baryon effects can solve all the small-scale problems.

Small-scale problems may indicate that our assumption for DM, i.e., collisionless, needs to be modified. As first pointed out in [15], a large elastic scattering cross section between DMs can solve the core-cusp and missing satellites problems. Since then, the DM self-interaction was studied by a series of works via N-body simulations [16–30]. Recent studies have shown that a constant cross-section between DM is not favored by simulation or semianalytical results. In a nutshell, in dwarf galaxies (where DM velocity $v_{\rm DM} \sim 10$–100 km/s) the cross section per unit mass $\sigma/m_{\rm DM}$ needs to be in the range $\mathcal{O}(1)$–$\mathcal{O}(10)$ cm^2/g to solve core-cusp and TBTF problems [26,27], but studies of galaxy groups ($v_{\rm DM} \sim 1000$ km/s) and galaxy clusters ($v_{\rm DM} \gtrsim 1500$ km/s) indicate $\sigma/m_{\rm DM} \sim 0.5$ and $\sigma/m_{\rm DM} \lesssim 0.1$ cm^2/g, respectively [31–36]. To be consistent with observables at different scales, a velocity dependent cross section is required [32]. See [37] for a recent review.

Introducing a light mediator which couples to DM seems to be the easiest way to generate the velocity dependent inter-DM cross section [32,38–65]. Such a scenario is favored in many aspects. For example, DM relic density can be realized via the so-called "secluded freeze-out" process [66], which means DM annihilates to light mediators instead of visible SM particles. And, because DM relic density and its coupling with SM are unbound, it is easier for such DM models to escape limits from direct detection or collider experiments [67–73]. However, other studies pointed out that such a "self-interacting DM with light mediator" scenario is strongly constrained by Big Bang nucleosynthesis (BBN), cosmic microwave background (CMB), and indirect search results [74–83]. This is because the Sommerfeld enhancement induced by the light mediator increases rapidly as DM velocity decreases in the expanding universe [84–90], and thus the energy injection from DM annihilation will affect observables (like BBN or CMB) even after DM freeze-out. Especially, the s-wave annihilation case (e.g., DM annihilates to dark gauge boson pair) has been fully excluded by CMB data [91].

A simple method to evade those constraints on DM annihilation is to consider the asymmetric dark matter (ADM). In the ADM scenario, DM is not neutral and

*Corresponding author.
mczhang@jnu.edu.cn

self-conjugate, but instead DM is conjugated to anti-DM and the observed DM relic density is determined by the asymmetry between DM and anti-DM. See [92–94] for a recent review. When the thermal bath temperature is much lower than the DM mass, the abundance of anti-DM has been reduced to negligible level. So, the annihilation between DM and anti-DM is much less constrained compared with the symmetric case [95,96]. Another advantage of the ADM model is that it helps to explain the "$\Omega_{\rm DM} \simeq 5\Omega_{\rm B}$" coincidence. See [97–128] for related studies.

In this work we study the DM self-interaction in a concise ADM model framework. Combining ADM and DM self-interaction is not a new idea, see, e.g., [129–137]. Compared with previous work, we only consider one flavor of DM (to be labeled as χ) which is charged under a dark $U(1)'$. In addition, we introduce two dark Higgs bosons (to be labeled as S_1 and S_2) charged under the same dark $U(1)'$. S_1 helps to generate the asymmetry in the dark sector and become dark radiation in the end, and S_2 is used to break $U(1)'$ and thus prohibit the long-range interaction between DMs. The reason for us to introduce two dark Higgs is that we do not want the troublesome Majorana dark matter mass to be induced by $U(1)'$ symmetry breaking. We will clarify this point in the next section. To simplify our analysis, we will consider a nearly independent dark sector. It means that the portal between the dark sector and visible sector is too weak for them to reach thermal equilibrium. And thus the portal is also difficult to be searched for via traditional methods like direct detection or collider experiment. However, the $U(1)'$ phase transition in the dark sector provides a possible method to detect the dark sector by gravitational waves (GWs), provided the phase transition is first order. In addition, dark radiation changes the value of the effective number of neutrinos ($N_{\rm eff}$), which makes this model detectable in the near future.

This paper is organized in the following way. In the next section, we introduce the model framework we want to study. In Sec. III we explain how to generate the asymmetry in the dark sector. We will also discuss the sequential thermal history and related constraints. Section IV is dedicated to the DM self-interacting and its consistency with data. In Sec. V we discuss the possibility to detect this model via gravitational waves. We conclude this work in Sec. VI.

II. MODEL FRAMEWORK

In this section we introduce the framework of our model, and specify the scenario we want to study.

A. Model introduction

We consider the SM model extended by a dark $U(1)'$ gauged sector. For similar model framework see Refs. [114,115,133,138]. The Lagrangian can be schematically expressed as

$$\mathcal{L} = \mathcal{L}_{\rm SM} + \mathcal{L}_{\rm Dark} + \mathcal{L}_{\rm Portal}, \tag{1}$$

where $\mathcal{L}_{\rm Dark}$ is the Lagrangian of a $U(1)'$ gauged dark sector. The dark sector includes a Dirac fermion χ [dark matter candidate charged under $U(1)'$], dark Higgs S_1 [has the same $U(1)'$ charge as χ], and dark Higgs S_2 [used to break $U(1)'$ at a later time]. The expression of $\mathcal{L}_{\rm Dark}$ is

$$\mathcal{L}_{\rm Dark} = \bar{\chi}(i\not{D} - m_\chi)\chi - (D_\mu S_1)^\dagger D^\mu S_1 - (D_\mu S_2)^\dagger D^\mu S_2 - \frac{1}{4}F'_{\mu\nu}F'^{\mu\nu} - V(S_1, S_2). \tag{2}$$

Here $D_\mu \equiv \partial_\mu + ig'Q_i A'_\mu$ $(i = \chi, S_1, S_2)$ is the covariant derivative, with g' and A'_μ being the dark gauge coupling and dark gauge boson, respectively. $U(1)'$ charge $\{Q_\chi, Q_{S_1}, Q_{S_2}\}$ are simply fixed to $\{+1, +1, +2\}$. $F'_{\mu\nu} \equiv \partial_\mu A'_\nu - \partial_\nu A'_\mu$ is the field strength of the dark gauge boson. And m_χ is the mass of dark matter given by hand. Dark scalar potential $V(S_1, S_2)$ is

$$V(S_1, S_2) = \mu_1^2 S_1^\dagger S_1 - \mu_2^2 S_2^\dagger S_2 + (\kappa S_2 S_1^\dagger S_1^\dagger + \text{H.c.}) + \frac{\lambda_1}{4}(S_1^\dagger S_1)^2 + \frac{\lambda_2}{4}(S_2^\dagger S_2)^2 + \lambda_{12}(S_1^\dagger S_1)(S_2^\dagger S_2). \tag{3}$$

S_2 needs to obtain a vacuum expectation value (VEV) after dark phase transition, and thus we insert a minus mass square term $-\mu_2^2$ for it. All possible triple and quartic dark Higgs interactions are given.

$\mathcal{L}_{\rm Portal}$ is the sector that connects the visible sector and dark sector, including Higgs portal, Abelian gauge boson kinetic mixing, and right-handed neutrino (RHN) portal. The general expression of $\mathcal{L}_{\rm Portal}$ is

$$\mathcal{L}_{\rm Portal} = \frac{1}{2}\sum_{i=1,2}\bar{N}_i(i\not{\partial} - M_{N_i})N_i^C - \sum_{i=1,2}\lambda_{S_iH}(S_i^\dagger S_i)(H^\dagger H) - \frac{1}{2}\epsilon F'_{\mu\nu}F^{\mu\nu} - \sum_{i=1,2}y'_i\bar{N}_i\chi S_1^\dagger - \sum_{i=1,2}y_i\bar{N}_i L H^\dagger + \text{H.c.} \tag{4}$$

Here λ_{S_iH} and ϵ are the coupling of Higgs portal and kinetic mixing parameter, respectively. Two Majorana RHN, N_1 and N_2, are introduced to generate the asymmetry in the dark or visible sector, with the help of complex phases of y'_i and y_i. L and H are the SM lepton doublet and Higgs doublet, respectively.

Now we explain the reason to introduce two dark Higgs S_1 and S_2. Assuming that there is no S_2 and $U(1)'$ is broken by VEV $\langle S_1\rangle$, then, by integrating out N_1, a Majorana DM mass ($\sim \frac{(y'_1\langle S_1\rangle)^2}{M_{N_1}}$) will be induced. This Majorana mass term

makes DM oscillate to anti-DM in the late universe. Thus the asymmetry in the dark sector will be partly erased, and our model will be more limited [139,140]. To make DM stable during the universe lifetime, M_{N_1} needs to be even higher than Planck scale. So, to forbid the annoying DM-anti-DM oscillation, in this work we introduce another dark Higgs S_2 to break $U(1)'$ and keep $\langle S_1 \rangle = 0$ all the way. However, it needs to be mentioned that coupling like $y_\chi S_2^\dagger \chi\chi + \text{H.c.}$ is also allowed by the $U(1)'$ gauge symmetry. And thus after S_2 obtaining VEV, Majorana mass appears again. Furthermore, $y_\chi S_2 \chi\chi$ combined with $\kappa S_2^\dagger S_1 S_1$ leads to additional washout of the generated DM asymmetry. The $\kappa S_2^\dagger S_1 S_1$ term also breaks the particle number conservation of S_1 in the late universe. To forbid troublesome couplings like $y_\chi S_2^\dagger \chi\chi$ or $\kappa S_2^\dagger S_1 S_1$, one can consider a different $U(1)'$ charge of S_2. For example, one can consider $Q_{S_2} = +5/2$ or $Q_{S_2} = +4$. The modification of Q_{S_2} does not have much impact on our following discussion and the main conclusion of this article.

B. Our scenario

The model we introduced above is nearly the minimal model that can generate matter asymmetry and induce velocity dependent DM self-interaction. However, even for such a nearly minimal model, there are still a dozen parameters to be fixed. Diverse and complex phenomena can occur in different parameter spaces, which is difficult to be covered in a single paper. Thus, in this paper we choose a simplified scenario to analyze, instead of studying the entire allowed parameter space.

The first simplification we will perform is neglecting $y_i \bar{N}_i L H^\dagger$, which is used to generate visible matter asymmetry. The inclusion of $y_i \bar{N}_i L H^\dagger$ inevitably entangle asymmetries in the dark sector and visible sector [115], and force us to consider the limits from neutrino data [133]. So, in order to focus on phenomena in the dark sector, we are temporarily agnostic to the baryon asymmetry problem and neglect $y_i \bar{N}_i L H^\dagger$.

Second, we require all the other portals' couplings, i.e., $\lambda_{S_1 H}$, $\lambda_{S_2 H}$, and ϵ, to be small enough to avoid current limits from terrestrial experiments. Furthermore, we also require that these portals are too weak to keep the dark sector and visible sector in the thermal equilibrium from reheating to current time. These requirements are made for simplicity. However, it is also important to study the detectability of this extreme scenario. As we will show later, stochastic GWs and the change of N_{eff} are possible detection methods.

III. THERMAL HISTORY OF THE DARK SECTOR AND ITS PARAMETER BOUNDS

Before the thermal history analysis, in Table I we present all the particles in the dark sector. Their mass range and the role they played are also given. The mass of dark matter (m_χ) and dark mediator ($m_{\gamma'}$) are chosen to be consistent with the small scale data. To generate asymmetry in the dark sector, the decay of N_1 needs to be out of equilibrium, and thus the mass of N_1 should be much larger than its decay products. The mass of s_2 [s_2 is the scalar component of S_2 after $U(1)'$ breaking] is chosen to be smaller than $m_{\gamma'}$. As we will explain later, this is necessary if the $U(1)'$ symmetry breaking is a first order phase transition. Finally, the entropy in the dark sector should go to some nearly massless particles long after DM-anti-DM annihilation, otherwise there will be overclosure problems [124]. So we require S_1 to be very light and serve as dark radiation.

TABLE I. Particle content in the dark sector, with their mass range and role given.

Name	Mass range	Role
χ	10 GeV–100 GeV	Dark matter
γ'	1 MeV–100 MeV	Mediator between DMs
N_1, N_2	$M_{N_i} \gg m_\chi$, $M_{N_2} > M_{N_1}$	Generate DM-anti-DM asymmetry
S_2	$m_{s_2} < m_{\gamma'}$	Break $U(1)'$ symmetry
S_1	$m_{S_1} \ll 1$ eV	Dark radiation

Furthermore, we define the ratio between dark sector temperature T' and visible sector temperature T:

$$\xi \equiv \frac{T'}{T}. \tag{5}$$

The value of ξ will be different in a different period. In this work we assume the dark sector and visible sector thermally decoupled very early, then these two sectors evolve independently. The temperature ratio ξ at the time when dark sector temperature T' is lower than M_{N_2} and higher than M_{N_1}, is labeled by ξ_{ini}, and we take it as an input parameter.

Comoving entropy densities in each sector are conserved, respectively. So the temperature ratio in a different period will be rescaled by the effective numbers of relativistic degrees of freedom (d.o.f.) in each sectors (to be labeled as $g'_\star$ and $g_\star$)[1] at that time:

$$\xi = \xi_{\text{ini}} \left(\frac{g_\star \cdot g'_{\star,\text{ini}}}{g'_\star \cdot g_{\star,\text{ini}}} \right)^{\frac{1}{3}}. \tag{6}$$

In this work we assume $g_{\star,\text{ini}}$ to be the SM value 106.75 [141]. For the dark sector, $g'_{\star,\text{ini}}$ comes from N_1, χ, S_1, S_2, and γ'. And so,

[1]Strictly speaking, $g_\star$ for energy density and entropy density are different. But before the neutrino decoupling, the relativistic d.o.f. for energy density and entropy density in the visible sector are the same.

$$g'_{\star,\mathrm{ini}} = \frac{7}{8}(2+4) + (2+2+2) = 11.25. \tag{7}$$

Given two initial values $g_{\star,\mathrm{ini}}$ and $g'_{\star,\mathrm{ini}}$, the temperature ratio ξ at a later time can be determined.

During the radiation dominant period, energy and entropy densities are given by

$$\begin{cases} \rho = \frac{\pi^2}{30}(g_\star/\xi^4 + g'_\star)T'^4 = \frac{\pi^2}{30} g_{\mathrm{eff}}(T')T'^4 \\ s = \frac{2\pi^2}{45}(g_\star/\xi^3 + g'_\star)T'^3 = \frac{2\pi^2}{45} h_{\mathrm{eff}}(T')T'^3. \end{cases} \tag{8}$$

Here we define the effective d.o.f. for energy and entropy, $g_{\mathrm{eff}}(T')$ and $h_{\mathrm{eff}}(T')$, for later convenience.

A. The generation of dark sector asymmetry

In this subsection we introduce the generation of $Y_{\Delta\chi} \equiv Y_\chi - Y_{\bar\chi}$. Here Y is the particle yield, which equals to particle number density divided by entropy density. Before the $U(1)'$ symmetry breaking, $U(1)'$ charge is conserved and thus $Y_{\Delta S_1} \equiv Y_{S_1} - Y_{S_1^\dagger} = -Y_{\Delta\chi}$. Similar to the vanilla leptogenesis [142–145], nonzero $Y_{\Delta\chi}$ is generated by the CP violated and out-of-equilibrium decay of N_1. See Fig. 1 for illustration.

Asymmetric yield $Y_{\Delta\chi}$ can be expressed as

$$Y_{\Delta\chi} = Y_{N_1} \times \epsilon \times \eta. \tag{9}$$

Here, Y_{N_1} is the yield of N_1 before it decays. Because N_1 is in the equilibrium with dark thermal bath initially, so the initial yield of N_1 is

$$\begin{aligned} Y_{N_1} &= \left(\frac{3}{4} 2 \frac{\zeta(3)}{\pi^2} T'^3\right) \div \left[\frac{2\pi^2}{45}(g'_{\star,\mathrm{ini}} T'^3 + g_{\star,\mathrm{ini}} T^3)\right] \\ &\simeq \frac{0.42}{11.25 + 106.75/\xi_{\mathrm{ini}}^3}. \end{aligned} \tag{10}$$

ϵ is the CP asymmetry generated by N_1 decay,

$$\epsilon \equiv \frac{\Gamma(N_1 \to \chi S_1^\dagger) - \Gamma(N_1 \to \bar\chi S_1)}{\Gamma(N_1 \to \chi S_1^\dagger) + \Gamma(N_1 \to \bar\chi S_1)}. \tag{11}$$

The expression of ϵ can be simplified when $M_{N_2} \gg M_{N_1}$. In this case, ϵ is approximately given by

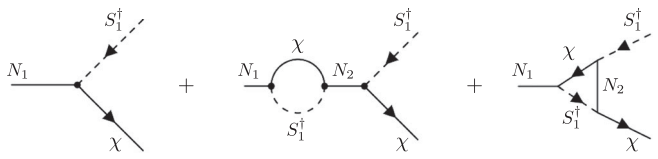

FIG. 1. CP violated process in the dark sector that generates the asymmetry between DM and anti-DM.

$$\epsilon \simeq -\frac{1}{16\pi}\frac{M_{N_1}}{M_{N_2}}\frac{\mathrm{Im}[(y'^*_2 y'_1)^2]}{|y'_1|^2}. \tag{12}$$

η is the efficiency factor that reduce the final generated asymmetry. In the so-called "weak washout" case where the decay width of N_1 is smaller than the Hubble expansion rate ($\Gamma_{N_1} < H(T' = M_{N_1})$), the value of η can be close to 1. To simplify our analysis we will only consider the weak washout case, and it leads to a constraint on the parameter space:

$$\Gamma_{N_1} < H(T' = M_{N_1}) \tag{13}$$

$$\Rightarrow \frac{|y'_1|^2}{16\pi} M_{N_1} < 1.66 \frac{M_{N_1}^2}{M_{\mathrm{Pl}}} \sqrt{g'_{\star,\mathrm{ini}} + g_{\star,\mathrm{ini}}/\xi_{\mathrm{ini}}^4} \tag{14}$$

$$\Rightarrow M_{N_1} > \frac{|y'_1|^2 M_{\mathrm{Pl}}}{83.44 \times \sqrt{11.25 + 106.75/\xi_{\mathrm{ini}}^4}}. \tag{15}$$

Here $M_{\mathrm{Pl}} \simeq 1.22 \times 10^{19}$ GeV is the Planck mass. So there is a large parameter space to satisfy the weak washout requirement if reheating temperature is high enough and $|y'_1|$ is small.

For convenience, we define the CP phase angle θ by

$$(y'^*_2 y'_1)^2 = |y'_2|^2 |y'_1|^2 e^{i\theta}. \tag{16}$$

In Fig. 2 we show $Y_{\Delta\chi}$ as functions of CP phase angle θ with $\frac{M_{N_1}}{M_{N_2}} = 0.1$ and ξ_{ini} fixed to 1, 0.5, and 0.1, respectively. It can be seen that even for very small ξ_{ini}, $Y_{\Delta\chi}$ can exceed 10^{-9}. DM relic density can be estimated by

$$\Omega_\chi h^2 \approx m_\chi Y_{\Delta\chi} s_0/\rho_{\mathrm{cr}} \approx Y_{\Delta\chi}\left(\frac{m_\chi}{\mathrm{GeV}}\right) \times 2.72 \times 10^8. \tag{17}$$

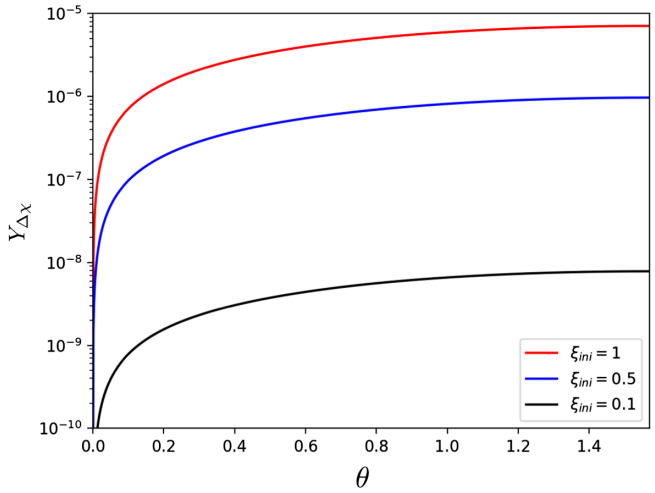

FIG. 2. $Y_{\Delta\chi} \equiv Y_\chi - Y_{\bar\chi}$ as functions of the CP phase angle θ with different ξ_{ini} values.

For dark matter mass m_χ larger than 10 GeV, it is always possible to explain the current observed relic density ($\Omega_\chi h^2 \approx 0.12$), provided $\xi_{\rm ini}$ is not much smaller than 1. So we can take $Y_{\Delta\chi}$ as an input parameter, which should be consistent with $\Omega_\chi h^2 \approx 0.12$, in the following analysis.

B. $\chi - \bar{\chi}$ annihilation

As we explained in the introduction, asymmetry DM helps to escape the limits from observations like CMB. To be more specific, compared with symmetric DM scenario, the energy injection rate in the ADM scenario during recombination is suppressed by the asymptotic ratio:

$$r_\infty = \frac{Y_{\bar{\chi}}(\infty)}{Y_\chi(\infty)}. \tag{18}$$

To obtain r_∞ (here "∞" corresponds to recombination time), we need to solve the following Boltzmann equations for yields Y_χ and $Y_{\bar{\chi}}$ [146–152]:

$$\frac{dY_{\chi,\bar{\chi}}}{dx} = -\frac{m_\chi M_{\rm Pl}}{x^2}\sqrt{\frac{\pi g_*}{45}}\langle\sigma_{\rm ann} v\rangle (Y_\chi Y_{\bar{\chi}} - Y_{\rm eq}^{\rm sym} Y_{\rm eq}^{\rm sym}). \tag{19}$$

Here, $x \equiv m_\chi/T'$, and $Y_{\rm eq}^{\rm sym}$ is the equilibrium yield of χ (or $\bar{\chi}$) with chemical potential being zero (correspond to the symmetric case):

$$Y_{\rm eq}^{\rm sym} = \left(\frac{2}{(2\pi)^3}\int \frac{d^3\vec{p}}{e^{\sqrt{m_\chi^2+\vec{p}^2}/T'}+1}\right) \div \left[\frac{2\pi^2}{45} h_{\rm eff}(T') T'^3\right]. \tag{20}$$

And,

$$\sqrt{g_*} = \frac{h_{\rm eff}}{\sqrt{g_{\rm eff}}}\left(1 + \frac{T'}{3h_{\rm eff}}\frac{dh_{\rm eff}}{dT'}\right). \tag{21}$$

Ratio $r(x)$ is a function of x, and the asymptotic ratio r_∞ is the value of $r(x)$ when $x \to \infty$:

$$r(x) = \frac{Y_{\bar{\chi}}(x)}{Y_\chi(x)}, \qquad r_\infty = \lim_{x\to\infty} r(x). \tag{22}$$

We follow the method proposed in [148,152] to calculate r_∞. For later convenience, first we need to define the equilibrium ratio $r_{\rm eq}(x)$ as

$$\begin{aligned} r_{\rm eq}(x) &= \frac{Y_{\rm eq}^{\rm sym} \times \exp\left[-\sinh^{-1}\left(\frac{Y_{\Delta\chi}}{2Y_{\rm eq}^{\rm sym}}\right)\right]}{Y_{\rm eq}^{\rm sym} \times \exp\left[+\sinh^{-1}\left(\frac{Y_{\Delta\chi}}{2Y_{\rm eq}^{\rm sym}}\right)\right]} \\ &= \exp\left[-2\sinh^{-1}\left(\frac{Y_{\Delta\chi}}{2Y_{\rm eq}^{\rm sym}}\right)\right]. \end{aligned} \tag{23}$$

Here, "$\sinh^{-1}(\frac{Y_{\Delta\chi}}{2Y_{\rm eq}^{\rm sym}})$" is actually the ratio between chemical potential and temperature. Then Boltzmann equations (19) can be transferred to a differential equation for $r(x)$ [148]:

$$\frac{dr}{dx} = -\frac{m_\chi M_{\rm Pl}}{x^2}\sqrt{\frac{\pi g_*}{45}}\langle\sigma_{\rm ann} v\rangle Y_{\Delta\chi}\left[r - r_{\rm eq}\left(\frac{1-r}{1-r_{\rm eq}}\right)^2\right]. \tag{24}$$

Before freeze-out ($x < x_{\rm FO}$), χ and $\bar{\chi}$ are in the thermal equilibrium and thus $r = r_{\rm eq}$. After freeze-out ($x > x_{\rm FO}$), $r_{\rm eq}$ decreases much faster than r and thus Eq. (24) can be approximatively simplified to

$$\frac{dr}{dx} \simeq -\frac{m_\chi M_{\rm Pl}}{x^2}\sqrt{\frac{\pi g_*}{45}}\langle\sigma_{\rm ann} v\rangle Y_{\Delta\chi} r. \tag{25}$$

Then we obtain the approximate expression of r_∞:

$$r_\infty \simeq r(x_{\rm FO}) \exp\left[-m_\chi M_{\rm Pl} Y_{\Delta\chi}\int_{x_{\rm FO}}^{\infty}\sqrt{\frac{\pi g_*}{45}}\frac{\langle\sigma_{\rm ann} v\rangle}{x^2}dx\right]. \tag{26}$$

At the freeze-out temperature ($x = x_{\rm FO}$), there is little difference between r and $r_{\rm eq}$. So Eq. (26) can be further simplified to

$$r_\infty \simeq r_{\rm eq}(x_{\rm FO}) \exp\left[-m_\chi M_{\rm Pl} Y_{\Delta\chi}\int_{x_{\rm FO}}^{\infty}\sqrt{\frac{\pi g_*}{45}}\frac{\langle\sigma_{\rm ann} v\rangle}{x^2}dx\right]. \tag{27}$$

Previous numerical study [152] shows that, for coupling strength $g'^2/4\pi \lesssim 0.1$, the inclusion of nonperturbative effects (i.e., Sommerfeld enhancement and bound state formation) is not important in the calculation of r_∞. Thus, we can approximately replace the cross section by its leading-order perturbative value when $g'^2/4\pi \lesssim 0.1$[2]:

$$(\sigma_{\rm ann} v) \simeq (\sigma_{\rm ann} v)_0 = \frac{\pi\alpha'^2}{m_\chi^2} Q_\chi^4. \tag{28}$$

Here $\alpha' \equiv g'^2/4\pi$ is the dark fine structure constant. And Q_χ has been fixed to 1 in this work. By this approximation, Eq. (27) is further simplified to

$$r_\infty \simeq r_{\rm eq}(x_{\rm FO}) \exp\left[-\frac{M_{\rm Pl} Y_{\Delta\chi}}{m_\chi}\sqrt{\frac{\pi^3}{45}}\alpha'^2\int_{x_{\rm FO}}^{\infty}\frac{\sqrt{g_*}}{x^2}dx\right]. \tag{29}$$

[2]For a larger value of $g'^2/4\pi$, the nonperturbative effects always cause r_∞ to be further suppressed. See [152] for detailed discussion.

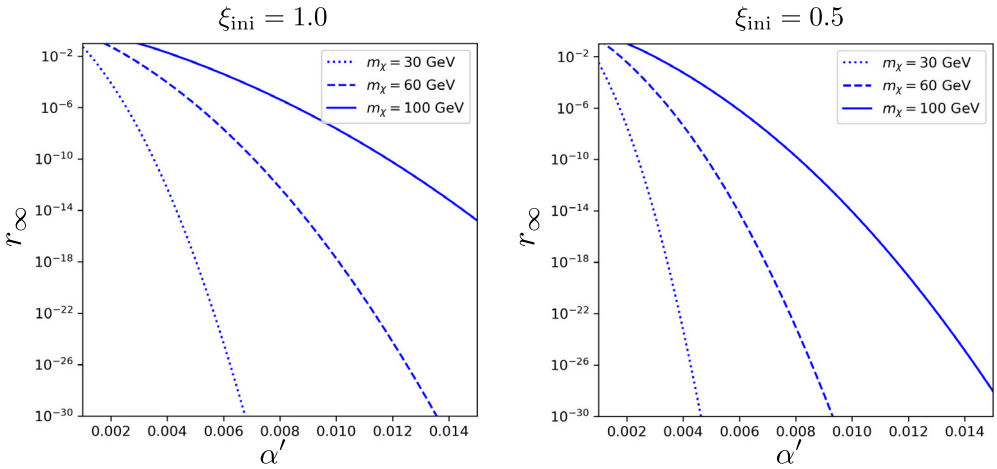

FIG. 3. r_∞ as functions of dark fine structure constant α', with different dark matter mass m_χ and different initial temperature ratio $\xi_{\rm ini}$.

Finally, freeze-out temperature is determined by

$$x_{\rm FO} - \frac{1}{2}\ln x_{\rm FO} \simeq \ln\left[0.076 \times m_\chi M_{\rm Pl}(\sigma_{\rm ann}v)_0 \frac{\sqrt{g_*^{\rm FO}}}{h_{\rm eff}^{\rm FO}}\right]. \quad (30)$$

With all the above information, we can estimate r_∞ numerically.

In Fig. 3 we present the value of r_∞ as functions of α'. It clearly shows that r_∞ is very sensitive to the value of α'. With α' increasing from $\mathcal{O}(0.001)$ to $\mathcal{O}(0.01)$, r_∞ decreases by more than 10 orders. The decreasing of r_∞ becomes much quicker for smaller dark matter mass. This trend is consistent with previous study [148]. We also present the dependence of r_∞ on temperature ratio, and our results show that r_∞ will be smaller if dark sector is colder than the visible sector. This relationship can be understood by the enhanced $\sqrt{g_*}$ during freeze-out when the dark sector becomes colder.

C. Limit on $\chi - \bar{\chi}$ annihilation during recombination

As we explained in the introduction, the strong limit of CMB data on dark matter annihilation during the recombination period can be greatly weakened by the asymmetry of dark matter. However, due to the scenario we have chosen to study in this work, this problem is "oversolved." In our scenario, we let S_1 to be nearly massless and serve as dark radiation. So the dominant decay channel of the mediator is $\gamma' \to S_1^\dagger S_1$, and the energy injection from $\chi - \bar{\chi}$ annihilation goes to the dark thermal bath instead of the visible sector. Thus the already formed neutral hydrogen atoms will not be reionized by a high energy electric shower, and $\chi - \bar{\chi}$ annihilation in our scenario is safe from the direct CMB limit.

But it is still very interesting to see how the DM asymmetry helps to weaken the CMB limit. So in this subsection we will deviate from our scenario and assume that the mediator mainly decays to electrons. In this case, BBN, supernova data, and direct detection give strong bounds on the mass and lifetime on $\mathcal{O}(1)$–$\mathcal{O}(10)$ MeV mediator (see, e.g., Refs. [153–157] for a detailed discussion). But here we will only focus on the CMB bound.

As we said in the last subsection, nonperturbative effects in the annihilation process can be ignored in the calculation of r_∞ for dark matter lighter than 100 GeV. But in the study of energy injection during recombination, including the nonperturbative effects in annihilation is important. Here we perform an approximate analysis like [91], which only include the Sommerfeld enhancement in the estimation of annihilation cross section during recombination period.

The annihilation cross section can be written as the tree-level cross section multiplied by a Sommerfeld enhancement factor [158]:

$$(\sigma_{\rm ann}v) = S(v) \times (\sigma_{\rm ann}v)_0. \quad (31)$$

Tree-level annihilation cross section $(\sigma_{\rm ann}v)_0 = \pi\alpha'^2 Q_\chi^4/m_\chi^2$ has been given in the previous subsection. Sommerfeld enhancement factor $S(v)$ is

$$S(v) = \frac{\pi}{\mathcal{A}(v)} \frac{\sinh(2\pi\mathcal{A}(v)\mathcal{B})}{\cosh(2\pi\mathcal{A}(v)\mathcal{B}) - \cos(2\pi\sqrt{\mathcal{B} - (\mathcal{A}(v)\mathcal{B})^2})} \quad (32)$$

with

$$\mathcal{A}(v) = \frac{v}{2Q_\chi^2\alpha'}, \qquad \mathcal{B} = \frac{6Q_\chi^2\alpha' m_\chi}{\pi^2 m_{\gamma'}}. \quad (33)$$

Sommerfeld enhancement factor will reach it maximal value, or say saturates, when velocity $v \lesssim m_{\gamma'}/2m_\chi$. During the recombination period, this saturation condition is already satisfied [91], and thus the annihilation cross section will generally be enhanced by several orders.

Many studies has been done on the CMB's constraints on dark matter annihilation [82,83,159,160]. A recent study [161] proposes a slightly stronger constraint by using combined data from Planck [162], BAO [163,164], and DES [165]. For electron final states and DM mass within 10 to 100 GeV, the limit on $\langle\sigma_{\rm ann}v\rangle_{\rm rec}/m_\chi$ is (for symmetric DM):

$$\frac{\langle\sigma_{\rm ann}v\rangle_{\rm rec}}{m_\chi}\lesssim 5\times10^{-28}\,{\rm cm^3\,s^{-1}\,GeV^{-1}}\ \ (4.26\times10^{-11}\,{\rm GeV^{-3}}). \tag{34}$$

Here we also give the limit in natural units. To illustrate how strong the CMB limit is, we can consider $\alpha'=0.01$ and $m_\chi=100$ GeV. In this case, $\frac{\langle\sigma_{\rm ann}v\rangle_{\rm rec}}{m_\chi}\sim S(v_{\rm rec})\times 10^{-10}\,{\rm GeV^{-3}}$. So even for $\mathcal{O}(1)$ enhancement factor $S(v_{\rm rec})$, this parameter choice cannot avoid CMB constraint. In the next section we will show that $\alpha'\sim\mathcal{O}(0.1)$ is generally required to solve the small scale problem. Thus, for symmetric DM, it is almost impossible to escape the CMB limit while explaining small scale data, provided the final state of DM annihilation is electron.

Different from the symmetric DM, in our ADM case, the CMB limit should be modified to [95,148,150]

$$\frac{2r_\infty}{(1+r_\infty)^2}\times\frac{\langle\sigma_{\rm ann}v\rangle_{\rm rec}}{m_\chi}\lesssim 5\times10^{-28}\ {\rm cm^3\,s^{-1}\,GeV^{-1}}\ (4.26\times10^{-11}\ {\rm GeV^{-3}}). \tag{35}$$

As we mentioned before, the energy injection from DM annihilation during recombination is reduced hugely by the small value of r_∞. And thus the constraint from CMB to dark sector parameters become much looser. In Fig. 4 we present the allowed parameter region with m_χ fixed to 100 and 60 GeV, respectively. As we have already shown in the last subsection, an increasing α' value lead to r_∞ exponential decreasing, and thus larger α' can more easily escape from CMB constraint. And for ADM mass within 10 to 100 GeV, $\alpha'\gtrsim0.01$ is large enough to escape the CMB limit (even if the final state of DM-anti-DM annihilation is electron). This is also favored by small scale data.

After the discussion of CMB constraint, we move back to our scenario with dark radiation.

D. Change of $N_{\rm eff}$

As we explain before, in our scenario all the entropy in the dark sector finally goes to nearly massless complex scalar S_1, which is the dark radiation. The presence of dark radiation will affect the measured value of the effective number of neutrino species $N_{\rm eff}$ [124]. $N_{\rm eff}$ is defined by the measured radiative energy density in addition to photon energy density:

$$\rho_r=\rho_\gamma\left[1+\frac{7}{8}\left(\frac{T_\nu}{T_\gamma}\right)^4N_{\rm eff}\right]. \tag{36}$$

Current constraint on $N_{\rm eff}$ from joint Planck + BAO data analysis is [166]

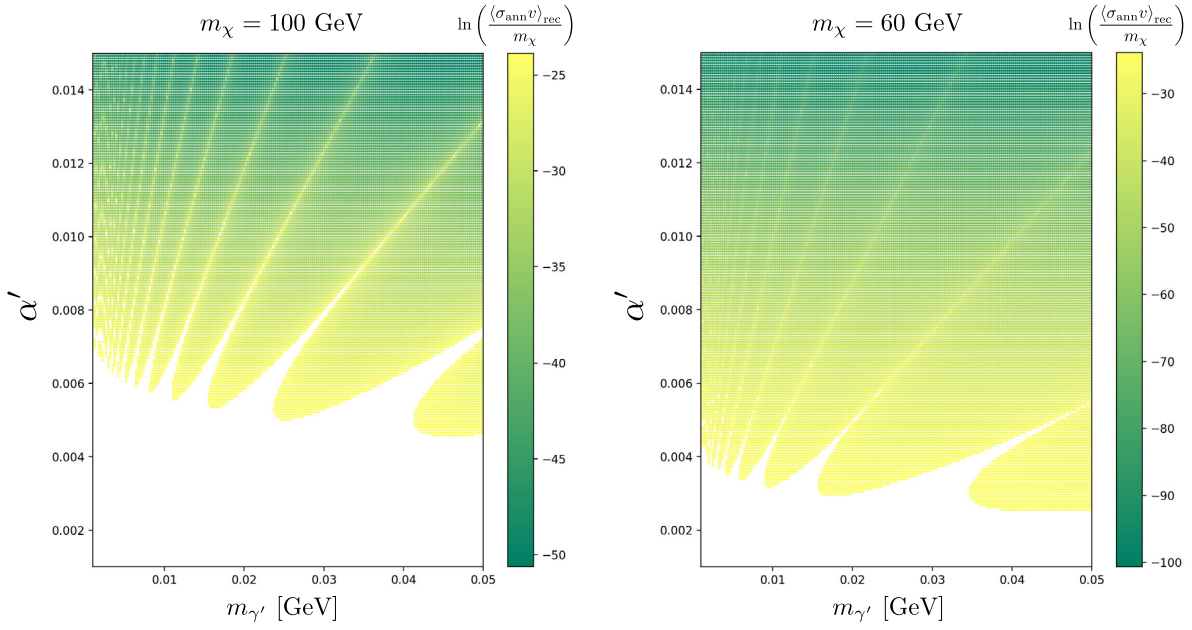

FIG. 4. CMB limit on the α'-$m_{\gamma'}$ plane with m_χ fixed to different values. In this plot we assume that the $\chi-\bar{\chi}$ annihilation mainly go to electron final states. The color indicates the natural logarithmic value of $\frac{\langle\sigma_{\rm ann}v\rangle_{\rm rec}}{m_\chi}$ in units of GeV^{-3}. The point with $\ln(\frac{\langle\sigma_{\rm ann}v\rangle_{\rm rec}}{m_\chi})>-23.88$ (blank region) have been excluded by current data.

$$N_{\rm eff} = 2.99^{+0.34}_{-0.33} \quad (95\%). \tag{37}$$

On the other hand, the SM prediction of $N_{\rm eff}$ is [167]

$$N_{\rm eff}^{\rm SM} = 3.045. \tag{38}$$

Thus there is a room about $\Delta N_{\rm eff} < 0.29$ for the existence of dark radiation (DR).

In this work we consider an independent dark sector, and hence T_ν/T_γ retain its SM value $(4/11)^{1/3}$. Then $\Delta N_{\rm eff}$ can be expressed as

$$\begin{aligned}\Delta N_{\rm eff} &= \frac{8}{7}\left(\frac{T_\nu}{T_\gamma}\right)^{-4}\frac{\rho_{\rm DR}}{\rho_\gamma} = \frac{8}{7}\left(\frac{4}{11}\right)^{-4/3}\left(\frac{2}{2}\right)\left(\frac{T'}{T_\gamma}\right)^4 \\ &= \frac{8}{7}\left(\frac{4}{11}\right)^{-4/3}\left(\frac{11.25\times 3.91}{106.75\times 2}\right)^{4/3}\xi_{\rm ini}^4.\end{aligned} \tag{39}$$

The temperature ratio T'/T_γ after the second equals sign should be estimated during the recombination period. Thus the limit on $\Delta N_{\rm eff}$ is transferred to the limit on $\xi_{\rm ini}$:

$$\xi_{\rm ini} < 0.86. \tag{40}$$

It should be noted that this up-limit on $\xi_{\rm ini}$ needs to be modified when the intensity of the dark $U(1)'$ phase transition is large [168]. We will discuss this point in the gravitational wave section.

The future CMB-S4 experiment will constrain the deviation from SM to $\Delta N_{\rm eff} < 0.06$ at 95% C.L. [169]. If the initial temperature ratio $\xi_{\rm ini}$ is not too small, then we should observe more than $\Delta N_{\rm eff}$ at CMB-S4.

E. Dark acoustic oscillations and collisional damping

The presence of dark radiation (DR) cause another problem which might make our scenario constrained by current cosmology observations. In our scenario, DM χ and DR S_1 are both charged under the $U(1)'$, and thus they can scatter with each other via the dark mediator γ'. This DM-DR scattering may cause the so-called "dark acoustic oscillations" (DAO) and the collisional (Silk) damping in the dark sector [170,171], provided the kinetic equilibrium between DM and DR lasts long enough. DAO and the collisional (Silk) damping will modify the initial matter power spectrum, and then leave imprints on CMB anisotropy and large scale structure (LSS) [170,171].

Reference [170] propose a parameter $\Sigma_{\rm DAO}$ as the proxy of this effect. $\Sigma_{\rm DAO}$ is related to the scattering cross section between DM and DR (labeled as $\sigma_{\text{DM-DR}}$) via

$$\frac{\sigma_{\text{DM-DR}}(T'_{\rm dec})}{m_\chi} = 1.9\times 10^{-4}\left(\frac{\xi_{\rm dec}}{0.5}\right)\left(\frac{\Sigma_{\rm DAO}}{10^{-3}}\right)\frac{\rm cm^2}{\rm g}, \tag{41}$$

where $T'_{\rm dec}$ is the DM kinetic decoupling temperature. $\sigma_{\text{DM-DR}}(T'_{\rm dec})$ and $\xi_{\rm dec}$ are scattering cross section and temperature ratio at $T'_{\rm dec}$, respectively. The bound on the value of $\Sigma_{\rm DAO}$ is $\Sigma_{\rm DAO} < 10^{-4.15}(10^{-3.6})$ for $\xi_{\rm dec} = 0.5$ (0.3) [170].

The kinetic decoupling temperature $T'_{\rm dec}$ is determined by

$$n_{\gamma'}\langle\sigma v\rangle_{\text{DM-DR}} v_{\rm DM}^2 \approx H(T'_{\rm dec}). \tag{42}$$

The left-hand side of the above equation can be approximated by

$$n_{\gamma'}\langle\sigma v\rangle_{\text{DM-DR}} v_{\rm DM}^2 \approx \frac{2.4}{\pi^2}(T'_{\rm dec})^3\times\pi\frac{\alpha'^2(T'_{\rm dec})^2}{m_{\gamma'}^4}\times\frac{T'_{\rm dec}}{m_\chi}. \tag{43}$$

Generally speaking, $T'_{\rm dec}$ is much smaller than $m_{\gamma'}$, so here we estimate $\langle\sigma v\rangle_{\text{DM-DR}}$ by a simple dimensional analysis. On the other hand, $H(T'_{\rm dec}) \approx 1.66\frac{(T'_{\rm dec})^2}{M_{\rm Pl}}\sqrt{2+3.4/\xi_{\rm dec}^4}$. Combined with Eq. (41) we can induce a bound on the dark sector coupling strength and spectrum (here we choose $\xi_{\rm dec} = 0.5$):

$$\frac{\alpha'}{m_{\gamma'}^2\sqrt{m_\chi M_{\rm Pl}}} \lesssim 4.7\times 10^{-3}\ {\rm GeV}^{-3}. \tag{44}$$

So it can be seen that even for $m_\chi = 10$ GeV and $m_{\gamma'} = 1$ MeV, the bound on α' is still very loose.

IV. DM SELF-INTERACTION AND SMALL SCALE STRUCTURE

In this section we investigate under which parameter settings the elastic scattering cross section between DMs can be consistent with small-scale observations. Parameters $\{m_\chi, m_{\gamma'}, \alpha'\}$ are relevant in this section.

The calculation methods of DM scattering cross section depend on the value of $\{m_\chi, m_{\gamma'}, \alpha'\}$ and the relative velocity between DMs. Basically, there are four different regimes. In the Born regime ($\frac{\alpha' m_\chi}{m_{\gamma'}} \ll 1$), one can do perturbative calculation and obtain the analytic formula directly [38,39,43,172]. In the classical regime ($\frac{\alpha' m_\chi}{m_{\gamma'}} \gtrsim 1$ and $\frac{m_\chi v_{\rm rel}}{m_{\gamma'}} \gg 1$), numerical results can be fitted with analytical functions [38,39,173,174]. In the quantum regime ($\frac{\alpha' m_\chi}{m_{\gamma'}} \gtrsim 1$ and $\frac{m_\chi v_{\rm rel}}{m_{\gamma'}} \lesssim 1$), the cross section can be estimated by using the Hulthén approximation [43]. Recently, the analytic formulas in the semiclassical regime ($\frac{\alpha' m_\chi}{m_{\gamma'}} \gtrsim 1$ and

TABLE II. Small scale data we considered to constrain DM scattering.

System	Scattering velocity $\langle v\rangle$	Required $\bar{\sigma}/m_\chi$
Dwarf galaxy/Galaxy	10–200 km/s	1–50 cm^2/g
Galaxy groups	1150 km/s	0.5 ± 0.2 cm^2/g
Galaxy clusters	1900 km/s	0.19 ± 0.09 cm^2/g

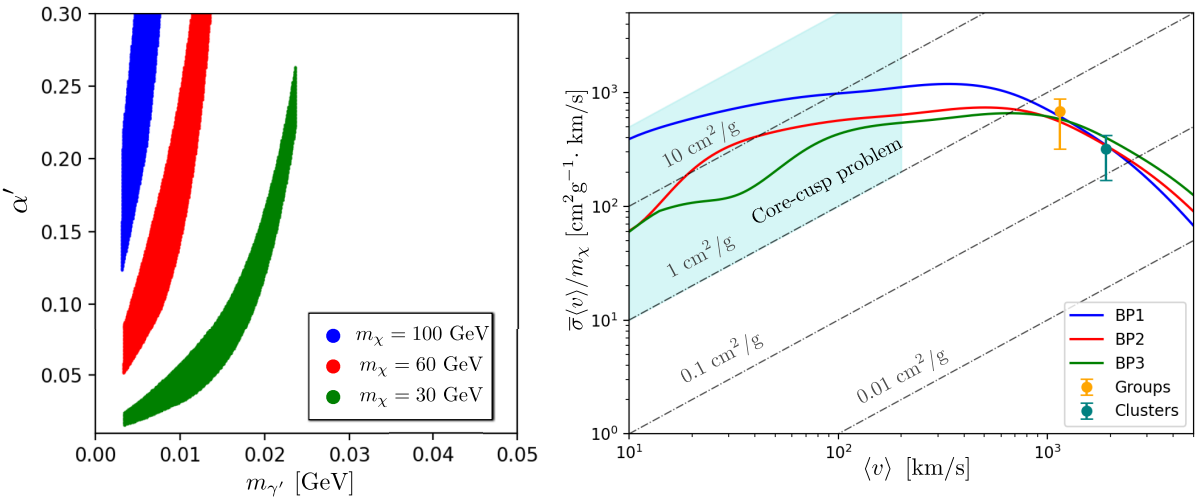

FIG. 5. Left: parameter region consistent with small scale data presented in Table II, with DM mass fixed to different values. Right: averaged elastic DM scattering cross section as functions of DM scattering velocity for three benchmark points.

$\frac{m_\chi v_{\rm rel}}{m_{\gamma'}} \gtrsim 1$) are also provided [175], which fills the gap between the quantum regime and classical regime.

In the literature, momentum transfer cross section $\sigma_{\rm T} \equiv \int d\Omega(1-\cos\theta)\frac{d\sigma}{d\Omega}$ is generally used as the proxy for DM elastic scattering. However, it is suggested to use viscosity cross section $\sigma_{\rm V} \equiv \int d\Omega \sin^2\theta \frac{d\sigma}{d\Omega}$ instead of $\sigma_{\rm T}$ as the proxy. Because $\sigma_{\rm V}$ is more related to the heat conductivity and $\sigma_{\rm V}$ is well defined for identical particles [43,175,176]. Reference [175] also suggests to use $\bar{\sigma} \equiv \langle \sigma_{\rm V} v_{\rm rel}^3 \rangle / 24\sqrt{\pi} v_0^3$ as the velocity averaged cross section, because this parameter is directly related to the energy transfer. All the above methods have been implemented in public code CLASSICS [175], and we will use this code to calculate the DM elastic scattering cross section in our model.

We list the observations we considered to constrain DM scattering in Table II. Fitting results for galaxy groups and clusters come from Ref. [34]. First, we perform a parameter scan with DM mass fixed to 100, 60, and 30 GeV, respectively. In the scan we require the calculated averaged cross section $\bar{\sigma}$, at different systems, to be within the ranges given in Table II. The scan results are present in Fig. 5 (left). It shows that for DM within mass range 10 GeV–100 GeV, $\alpha' \sim \mathcal{O}(0.1)$ and $m_{\gamma'} \sim \mathcal{O}(1)$ MeV–$\mathcal{O}(10)$ MeV are favored by small scale structure data. Coupling strength and mediator mass tend to decrease and increase, respectively, as DM becomes lighter. Furthermore, we choose three benchmark points to show the dependence of $\bar{\sigma}/m_\chi$ on scattering velocity:

$$\begin{aligned} &\text{Benchmark point 1:}\ m_\chi = 100\ \text{GeV}, \quad m_{\gamma'} = 3.5\ \text{MeV}, \quad \alpha' = 0.15, \\ &\text{Benchmark point 2:}\ m_\chi = 60\ \text{GeV}, \quad m_{\gamma'} = 7\ \text{MeV}, \quad \alpha' = 0.1, \\ &\text{Benchmark point 3:}\ m_\chi = 30\ \text{GeV}, \quad m_{\gamma'} = 12\ \text{MeV}, \quad \alpha' = 0.05. \end{aligned} \tag{45}$$

In Fig. 5 (right) we present scattering cross section as functions of $\langle v\rangle$ for these three benchmark points. It shows a clear velocity dependence that fits the data.

V. STOCHASTIC GRAVITATIONAL WAVES SIGNAL FROM THE DARK $U(1)'$ PHASE TRANSITION

So for, we have built up a model framework of ADM that is consistent with all the limits and can solve the small scale problems at the same time. We also pointed out that our scenario can be detected indirectly by the future precise $N_{\rm eff}$ measurement. In this section we discuss another detection method of this scenario.

Due to the nearly negligible portal between dark sector and visible sector in the scenario we have chosen in this work, traditional methods are powerless in detecting this scenario. But, if the spontaneous breaking of dark $U(1)'$ is induced by first order phase transition, then it is possible to detect the nearly independent dark sector by the stochastic gravitational wave signal [177–197]. Here we perform a brief analysis.

The sector related to the MeV scale dark $U(1)'$ symmetry breaking is generally called the Abelian Higgs model in the

literature [198,199]. Lattice simulation has already shown that the phase transition of the Abelian Higgs model is first order, provided the Higgs mass is smaller or much smaller than gauge boson mass [200,201]. The corresponding Lagrangian is given by

$$\mathcal{L}_{U(1)'} = -(\partial_\mu S_2 + i2g' A'_\mu S_2)^\dagger(\partial^\mu S_2 + i2g' A'^\mu S_2) - \frac{1}{4}F'_{\mu\nu}F'^{\mu\nu} + \mu_2^2 S_2^\dagger S_2 - \frac{\lambda_2}{4}(S_2^\dagger S_2)^2. \quad (46)$$

Here we do not need to include χ and S_1 because their masses are far from MeV scale. The $U(1)'$ charge of S_2 has been fixed to $+2$ as we said in Sec. II.

After S_2 got VEV, it can be expressed as

$$S_2 = \frac{1}{\sqrt{2}}(v + s_2 + ia). \quad (47)$$

Here $v \equiv 2\mu_2/\sqrt{\lambda_2}$ is the VEV of S_2 at zero temperature. s_2 and a are the scalar and pseudoscalar components of S_2, respectively. In the R_ξ gauge, the gauge fixing and ghost terms are

$$\mathcal{L}_{\mathrm{gf+gh}} = -\frac{1}{2}\xi^{-1}(\partial_\mu A^\mu - \xi 2g' v a)^2 - \bar{c}(-\partial_\mu\partial^\mu + \xi(2g')^2 v(v + s_2))c, \quad (48)$$

where c is the Grassmann ghost field. Zero temperature spectrums are given by

$$m_{s_2}^2 = \frac{1}{2}\lambda_2 v^2, \qquad m_a^2 = \xi(2g')^2 v^2, \qquad m_c^2 = \xi(2g')^2 v^2, \qquad m_{\gamma'}^2 = (2g')^2 v^2. \quad (49)$$

At finite temperature, S_2 field value $\phi \neq v$, and ϕ dependent spectrums are

$$m_{s_2}^2(\phi) = \frac{3}{4}\lambda_2\phi^2 - \mu_2^2, \quad m_a^2(\phi) = \frac{1}{4}\lambda_2\phi^2 - \mu_2^2 + \xi(2g')^2\phi^2, \quad m_c^2(\phi) = \xi(2g')^2\phi^2, \quad m_{\gamma'}^2(\phi) = (2g')^2\phi^2. \quad (50)$$

In the rest of this section we will consider the Landau gauge ($\xi = 0$) to decouple ghost fields. $\{m_{s_2}, m_{\gamma'}, \alpha'\}$ are chosen as input parameters to induce other relevant parameters.

A. Thermal effective potential

Free energy density of the dark $U(1)'$ sector is the thermal effective potential. The thermal effective potential at temperature[3] T can be schematically expressed as

$$V(\phi, T) = V^0(\phi) + V^{1-\mathrm{loop}}(\phi) + V^{\mathrm{T}}(\phi, T) + V^{\mathrm{daisy}}(\phi, T). \quad (51)$$

Here V^0 is the tree-level potential, $V^{1-\mathrm{loop}}$ is the sum of one-loop Coleman-Weinberg potential and counterterms, V^T is the thermal correction, and V^{daisy} is the correction from daisy resummation.

The tree-level potential comes from the potential sector of Lagrangian (46) by replacing S_2 by $\phi/\sqrt{2}$:

$$V^0(\phi) = -\frac{1}{2}\mu_2^2\phi^2 + \frac{1}{16}\lambda_2\phi^4. \quad (52)$$

The $V^{1-\mathrm{loop}}$ is composed by one-loop Coleman-Weinberg potential and counterterms, where the Coleman-Weinberg potential under the $\overline{\mathrm{MS}}$ renormalization scheme is [202]:

$$V^{\mathrm{CW}}(\phi) = \frac{1}{64\pi^2}\left\{ m_{s_2}^4(\phi)\left[\ln\left(\frac{m_{s_2}^2(\phi)}{Q^2}\right) - \frac{3}{2}\right] + m_a^4(\phi)\left[\ln\left(\frac{m_a^2(\phi)}{Q^2}\right) - \frac{3}{2}\right] + 3m_{\gamma'}^4(\phi)\left[\ln\left(\frac{m_{\gamma'}^2(\phi)}{Q^2}\right) - \frac{5}{6}\right]\right\}. \quad (53)$$

Here we need to emphasize that the potential parameter μ_2^2 and λ_2 is determined by input physical parameters $\{m_{s_2}, m_{\gamma'}, \alpha'\}$ via tree-level relation Eq. (49). Thus, to prevent physical mass and VEV being shifted by one-loop correction, counterterms need to be added to obey the following on-shell conditions:

$$\frac{d}{d\phi}\Delta V_1(\phi)\Big|_{\phi=v} = 0, \qquad \frac{d^2}{d\phi^2}\Delta V_1(\phi)\Big|_{\phi=v} = -\Delta\Sigma, \quad (54)$$

where $\Delta\Sigma \equiv \Sigma(m_{s_2}^2) - \Sigma(0)$ is the difference between scalar self-energy at different momentums. If all the involved particles are massive, it is harmless to ignore $\Delta\Sigma$ in Eq. (54). But Goldstone a in the Landau gauge is massless, and it causes an infrared (IR) divergence when we perform on-shell conditions on the Coleman-Weinberg potential. So we need the IR divergence in $\Delta\Sigma$ to make all IR divergences from Goldstone cancel out. See [203] for more detailed discussion. The one-loop correction which satisfies (54) is [204]:

[3]In this section, all the temperature labels represent dark sector temperature by default.

$$V^{1-\text{loop}}(\phi) = \frac{1}{64\pi^2}\left[m_{s_2}^4(\phi)\left(\ln\frac{m_{s_2}^2(\phi)}{m_{s_2}^2} - \frac{3}{2}\right) + 2m_{s_2}^2 m_{s_2}^2(\phi)\right] + \frac{3}{64\pi^2}\left[m_{\gamma'}^4(\phi)\left(\ln\frac{m_{\gamma'}^2(\phi)}{m_{\gamma'}^2} - \frac{3}{2}\right) + 2m_{\gamma'}^2 m_{\gamma'}^2(\phi)\right] + \frac{1}{64\pi^2}\left[m_a^4(\phi)\left(\ln\frac{m_a^2(\phi)}{m_{s_2}^2} - \frac{3}{2}\right)\right]. \tag{55}$$

The thermal correction is [205,206]

$$V^{\text{T}}(\phi, T) = \frac{T'^4}{2\pi^2}\left[J_B\left(\frac{m_{s_2}^2(\phi)}{T^2}\right) + J_B\left(\frac{m_a^2(\phi)}{T^2}\right) + 3J_B\left(\frac{m_{\gamma'}^2(\phi)}{T^2}\right)\right]. \tag{56}$$

Here the bosonic thermal function J_B is given by

$$J_B(x) = \int_0^\infty k^2 \ln\left[1 - \exp\left(-\sqrt{k^2 + x}\right)\right]dk. \tag{57}$$

To avoid the IR divergence when the mass of the boson is much smaller than temperature, daisy resummation needs to be added for the scalar and longitudinal component of γ' [207]:

$$V^{\text{daisy}}(\phi, T) = -\frac{T}{12\pi}\left\{\left[\left(m_{s_2}^2(\phi) + \Pi_{s_2}(T)\right)^{\frac{3}{2}} - \left(m_{s_2}^2(\phi)\right)^{\frac{3}{2}}\right] + \left[\left(m_a^2(\phi) + \Pi_a(T)\right)^{\frac{3}{2}} - \left(m_a^2(\phi)\right)^{\frac{3}{2}}\right] + \left[\left(m_{\gamma'}^2(\phi) + \Pi_{\gamma'}(T)\right)^{\frac{3}{2}} - \left(m_{\gamma'}^2(\phi)\right)^{\frac{3}{2}}\right]\right\}, \tag{58}$$

where $\Pi_{s_2}(T) = (\lambda_2/6 + (2g')^2/4)T^2$, $\Pi_a(T) = (\lambda_2/6 + (2g')^2/4)T^2$, and $\Pi_{\gamma'}(T) = ((2g')^2/3)T^2$ are thermal Debye mass squares.

B. Nucleation temperature

When the temperature is below the critical temperature, false vacuum transfer to true vacuum via thermal fluctuation.[4] The transition rate per unit volume is given by [208–210]

$$\Gamma(T) = A(T)e^{-S_E(T)}. \tag{59}$$

Here $A(T) = \omega T^4$ with $\omega \sim \mathcal{O}(1)$, and $S_E(T)$ is the 4D Euclidean action. In the case of thermal transition, $S_E(T)$ is the ratio between 3D Euclidean action $S_3(T)$ and temperature:

$$S_E(T) = \frac{S_3(T)}{T}. \tag{60}$$

And 3D Euclidean action $S_3(T)$ is given by

$$S_3(T) = \int d^3x\left[\frac{1}{2}(\nabla\phi)^2 + V(\phi, T)\right]. \tag{61}$$

Due to the 3D rotation invariance, ϕ only depend on radius r and thus S_3 can be rewritten as

$$S_3(T) = 4\pi\int_0^\infty r^2 dr\left[\frac{1}{2}\left(\frac{d\phi}{dr}\right)^2 + V(\phi, T)\right]. \tag{62}$$

Minimization condition of $S_3(T)$ gives the equation of motion that ϕ should follow:

$$\frac{d^2\phi}{dr^2} + \frac{2}{r}\frac{d\phi}{dr} = \frac{\partial V(\phi, T)}{\partial\phi}. \tag{63}$$

Adding boundary conditions $\lim_{r\to\infty}\phi(r) = 0$ and $\frac{d\phi}{dr}|_{r=0} = 0$, Eq. (63) can be solved numerically by the overshoot/undershoot method [211]. In this work we use public code CosmoTransitions [212] to do the calculation.

Nucleation starts at the temperature where the transition rate within one Hubble volume approximates the Hubble rate:

$$\begin{aligned} &H(T_N)^{-3} \times \Gamma(T_N) \approx H(T_N) \\ \Rightarrow\ &A(T_N)e^{-S_3(T_N)/T_N} \approx \left(1.66\frac{T_N^2}{M_{\text{Pl}}}\right)^4 (g_\star/\xi^4 + g'_\star)^2 \\ \Rightarrow\ &\frac{S_3(T_N)}{T_N} \approx 4\ln\left(\frac{M_{\text{Pl}}}{T_N}\right) - 2\ln(g_\star/\xi^4 + g'_\star) - 2.027. \end{aligned} \tag{64}$$

[4] In the case of the dark sector being much colder than the visible sector, quantum tunneling also needs to be considered. See Ref. [187] for a detailed discussion.

TABLE III. Benchmark points we considered for first order phase transition study.

Benchmark point	m_χ (GeV)	$m_{\gamma'}$ (MeV)	m_{s_2} (MeV)	α'	$\xi_{\rm ini}$	T_N (MeV)
BP1	100	3.5	1.5	0.15	0.7	1.63
BP2	60	7	2.5	0.1	0.7	1.83
BP3	30	12	3.8	0.05	0.7	3.75

Here T_N is the nucleation temperature, and we approximate ω to 1 in the third line. In our model, phase transition in the dark $U(1)'$ sector happens around the MeV scale, and the temperature ratio ξ is generally not much smaller than 1. So the nucleation temperature T_N is approximately determined by $S_3(T_N)/T_N \approx 196$.

In Table III we present three benchmark points we will study in this section. Initial temperature ratios $\xi_{\rm ini}$ are all fixed to 0.7 to be consistent with $N_{\rm eff}$ limit. Nucleation temperatures are determined by $S_3(T_N)/T_N \approx 196$. These three benchmark points are also consistent with small scale structure data.

C. Phase transition parameters

After nucleation, bubbles expand rapidly and after a while collide with each other and generate gravitational waves (GWs). There are three GW generation mechanisms: bubble walls collision [213–218], sound waves [219–222], and magnetohydrodynamic turbulence [223–228]. The generated gravitational waves stay in the universe and redshift in wavelength as the universe expands. To obtain the current spectrum of these phase transition gravitational waves, first we need to calculate a set of parameters used to describe the phase transition dynamics: T_*, $\mathbb{A}$,[5] $\mathbb{A}'$ ($\mathbb{A}$ in dark sector), β/H_*, v_w, and $\kappa_{b,s,t}$. The meaning of these parameters are given below.

T_* is the characteristic temperature of the GW generation. Generally, T_* can be chosen as the percolation temperature, the temperature at which a large fraction of the space has been occupied by bubbles [229–231]. But in the weak or mild supercooling case, using nucleation temperature T_N as T_* is also a good approximation. For the benchmark points we will study in this section, it is fine to approximate T_* by T_N because of the mild supercooling.

Strength parameter $\mathbb{A}$ is the change in the trace of the energy-momentum tensor during phase transition divided by relativistic energy density

$$\mathbb{A} = \frac{1}{\rho_*}\left[\Delta V - \frac{T}{4}\frac{d\Delta V}{dT}\right]_{T=T_*}. \tag{65}$$

[5]To avoid confusion with the label of fine structure constant, in this paper we use $\mathbb{A}$ to represent the strength parameter.

Here ρ_* is the relativistic energy density at T_*. ΔV is the difference in free energy density between false vacuum and true vacuum.

It will be convenient to study dark sector dynamics if we define another strength parameter $\mathbb{A}'$ by only considering the relativistic energy density in the dark sector [187]:

$$\mathbb{A}' = \frac{1}{\rho'_*}\left[\Delta V - \frac{T}{4}\frac{d\Delta V}{dT}\right]_{T=T_*} = \frac{\rho_*}{\rho'_*}\mathbb{A}. \tag{66}$$

Here ρ'_* is the relativistic energy density in the dark sector at T_*.

β is the inverse of the duration of phase transition. Its ratio to Hubble expansion rate at T_* is given by

$$\frac{\beta}{H_*} = T_*\left.\frac{dS_E}{dT}\right|_{T=T_*}. \tag{67}$$

v_w is the velocity of the bubble wall. $\kappa_{b,s,t}$ are the fractions of released vacuum energy that transferred to scalar-field gradients, sound waves, and turbulence, respectively. Before estimating these parameters, we need to judge whether the phase transition is "runaway" or "nonrunaway." To do that, first we calculate the so-called threshold value of $\mathbb{A}'$, which is labeled as $\mathbb{A}'_\infty$ [232]:

$$\mathbb{A}'_\infty = \frac{1}{\rho'_*}\frac{T_*^2}{24}\left(\sum_i c_i n_i \Delta m_i^2\right). \tag{68}$$

Here $c_i = 1(1/2)$ for bosons (fermions), n_i is the number of degrees of freedom (absolute value), and Δm_i^2 is the difference in particle mass square between false vacuum and true vacuum.

If $\mathbb{A}' > \mathbb{A}'_\infty$, the driving pressure will be larger than the friction from dark plasma and thus the bubble wall will eventually be accelerated to the maximal value, i.e., $v_w = 1$. This is the so-called runaway case. In this case, fractions $\kappa_{b,s,t}$ are given by [222,233][6]

$$\kappa_b = 1 - \frac{\mathbb{A}'_\infty}{\mathbb{A}'}, \qquad \kappa_s = \frac{\mathbb{A}'_\infty}{\mathbb{A}'}\frac{\mathbb{A}'_\infty}{0.73 + 0.083\sqrt{\mathbb{A}'_\infty} + \mathbb{A}'_\infty},$$
$$\kappa_t = 0.1\kappa_s. \tag{69}$$

If $\mathbb{A}' < \mathbb{A}'_\infty$, the bubble wall will eventually reach a subluminal velocity and this is called nonrunaway phase transition. In this case we simply choose $v_w = 0.9$ for a fast

[6]However, it should be noted that, as pointed out in [234], the ultrarelativistic bubble wall will produce soft gauge bosons and thus might change the final GWs spectrum. This is still an open question in the literature.

TABLE IV. Phase transition parameters.

Benchmark point	T_N (MeV)	$\mathbb{A}$	$\mathbb{A}'$	$\mathbb{A}'_\infty$	β/H_*	v_w	κ_b	κ_s	κ_t
BP1	1.63	3.20×10^{-4}	0.0234	0.410	3378.9	0.9	0	0.0305	0.00305
BP2	1.83	1.61×10^{-3}	0.117	1.05	784.7	0.9	0	0.134	0.0134
BP3	3.75	1.79×10^{-3}	0.131	0.657	2060.8	0.9	0	0.147	0.0147

and rough estimation of the GWs signal.[7] For the nonrunaway phase transition, the main source of GWs will be sound waves and the contribution from bubble collision is negligible. Fractions $\kappa_{b,s,t}$ are approximately given by [232] (here we use the expression for the highly relativistic bubble wall as an approximation):

$$\kappa_b \simeq 0, \qquad \kappa_s = \frac{\mathbb{A}'}{0.73 + 0.083\sqrt{\mathbb{A}'} + \mathbb{A}'}, \qquad \kappa_t = 0.1\kappa_s. \tag{70}$$

In Table IV we present all the phase transition parameters for the three benchmark points.

D. Gravitational waves

In this subsection we present the calculation of today's GWs signal in our model. Formulas used in this subsection can be found in the literature [218,222,228,242,243].

The total GWs signal is the linear superposition of spectrums from bubble collisions, sound waves, and turbulence:

$$h^2\Omega_{\rm GW}(f) = h^2\Omega_b(f) + h^2\Omega_s(f) + h^2\Omega_t(f). \tag{71}$$

The three individual contributions can be further divided into peak amplitudes ($\Omega^{\rm peak}_{b,s,t}$) and spectral shape functions ($\mathcal{S}_{b,s,t}$):

$$\begin{aligned} h^2\Omega_b(f) &\simeq h^2\Omega_b^{\rm peak}\mathcal{S}_b(f, f_b^{\rm peak}),\\ h^2\Omega_s(f) &\simeq h^2\Omega_s^{\rm peak}\mathcal{S}_s(f, f_s^{\rm peak}),\\ h^2\Omega_t(f) &\simeq h^2\Omega_t^{\rm peak}\mathcal{S}_t(f, f_t^{\rm peak}). \end{aligned} \tag{72}$$

Peak amplitudes are determined by all the phase transition parameters we obtained before:

$$\begin{aligned} h^2\Omega_b^{\rm peak} &= 1.24\times10^{-5}\left(\frac{h_{\rm eff0}}{h_{\rm eff*}}\right)^{4/3}(g_{\rm eff*})(\xi_0)^4\left(\frac{0.11v_w}{0.42+v_w^2}\right)\left(\frac{\kappa_b\mathbb{A}}{1+\mathbb{A}}\right)^2\left(\frac{v_w}{\beta/H_*}\right)^2,\\ h^2\Omega_s^{\rm peak} &= 1.97\times10^{-6}\left(\frac{h_{\rm eff0}}{h_{\rm eff*}}\right)^{4/3}(g_{\rm eff*})(\xi_0)^4\left(\frac{\kappa_s\mathbb{A}}{1+\mathbb{A}}\right)^2\left(\frac{v_w}{\beta/H_*}\right),\\ h^2\Omega_t^{\rm peak} &= 2.49\times10^{-4}\left(\frac{h_{\rm eff0}}{h_{\rm eff*}}\right)^{4/3}(g_{\rm eff*})(\xi_0)^4\left(\frac{\kappa_t\mathbb{A}}{1+\mathbb{A}}\right)^{3/2}\left(\frac{v_w}{\beta/H_*}\right), \end{aligned} \tag{73}$$

where "$*$" and "0" correspond to GWs producing time and current time, respectively. These formulas look different from expressions commonly found in the literature, because we need to recalculate the redshift factor for the MeV scale dark phase transition [186]. For our benchmark points, the factor inside the above expressions can be approximated to

$$\left(\frac{h_{\rm eff0}}{h_{\rm eff*}}\right)^{4/3}(g_{\rm eff*})(\xi_0)^4 \simeq \left(\frac{58.7}{173.2}\right)^{4/3}\times 424.0\times(0.41)^4 = 2.83. \tag{74}$$

[7]The calculation of v_w in a concrete model is still quite difficult. See Refs. [235–241] for previous studies.

Spectral shape functions are given by

$$\mathcal{S}_b(f, f_b^{\text{peak}}) = \left(\frac{f}{f_b^{\text{peak}}}\right)^{2.8}\left[\frac{3.8}{1+2.8(f/f_b^{\text{peak}})^{3.8}}\right],$$
$$\mathcal{S}_s(f, f_s^{\text{peak}}) = \left(\frac{f}{f_s^{\text{peak}}}\right)^{3}\left[\frac{7}{4+3(f/f_s^{\text{peak}})^{2}}\right]^{7/2},$$
$$\mathcal{S}_t(f, f_t^{\text{peak}}) = \left(\frac{f}{f_t^{\text{peak}}}\right)^{3}\left[\frac{1}{1+(f/f_t^{\text{peak}})}\right]^{11/3}\frac{1}{1+8\pi f/h_*}, \tag{75}$$

where

$$h_* = \frac{a_*}{a_0}H_* = 7.44\times10^{-11}\ \text{Hz}\left(\frac{g_{\text{eff}*}^{1/2}}{h_{\text{eff}*}^{1/3}}\right)\left(\frac{h_{\text{eff}0}}{3.91}\right)^{1/3} \times \xi_0\left(\frac{T_*}{1\ \text{MeV}}\right). \tag{76}$$

Here 3.91 is the current d.o.f. for entropy in the visible sector. For the MeV scale dark phase transition in our model, the value of h_* can be approximated to

$$h_* \simeq 2.78\times10^{-10}\ \text{Hz}\left(\frac{T_*}{1\ \text{MeV}}\right). \tag{77}$$

And peak frequencies are given by

$$f_b^{\text{peak}} = 7.44\times10^{-11}\ \text{Hz}\left(\frac{g_{\text{eff}*}^{1/2}}{h_{\text{eff}*}^{1/3}}\right)\left(\frac{h_{\text{eff}0}}{3.91}\right)^{1/3}\xi_0\left(\frac{T_*}{1\ \text{MeV}}\right)\left(\frac{\beta/H_*}{v_w}\right)\left(\frac{0.62v_w}{1.8-0.1v_w+v_w^2}\right)$$
$$\simeq 2.78\times10^{-10}\ \text{Hz}\left(\frac{T_*}{1\ \text{MeV}}\right)\left(\frac{\beta/H_*}{v_w}\right)\left(\frac{0.62v_w}{1.8-0.1v_w+v_w^2}\right), \tag{78}$$

$$f_s^{\text{peak}} = 8.59\times10^{-11}\ \text{Hz}\left(\frac{g_{\text{eff}*}^{1/2}}{h_{\text{eff}*}^{1/3}}\right)\left(\frac{h_{\text{eff}0}}{3.91}\right)^{1/3}\xi_0\left(\frac{T_*}{1\ \text{MeV}}\right)\left(\frac{\beta/H_*}{v_w}\right)$$
$$\simeq 3.21\times10^{-10}\ \text{Hz}\left(\frac{T_*}{1\ \text{MeV}}\right)\left(\frac{\beta/H_*}{v_w}\right), \tag{79}$$

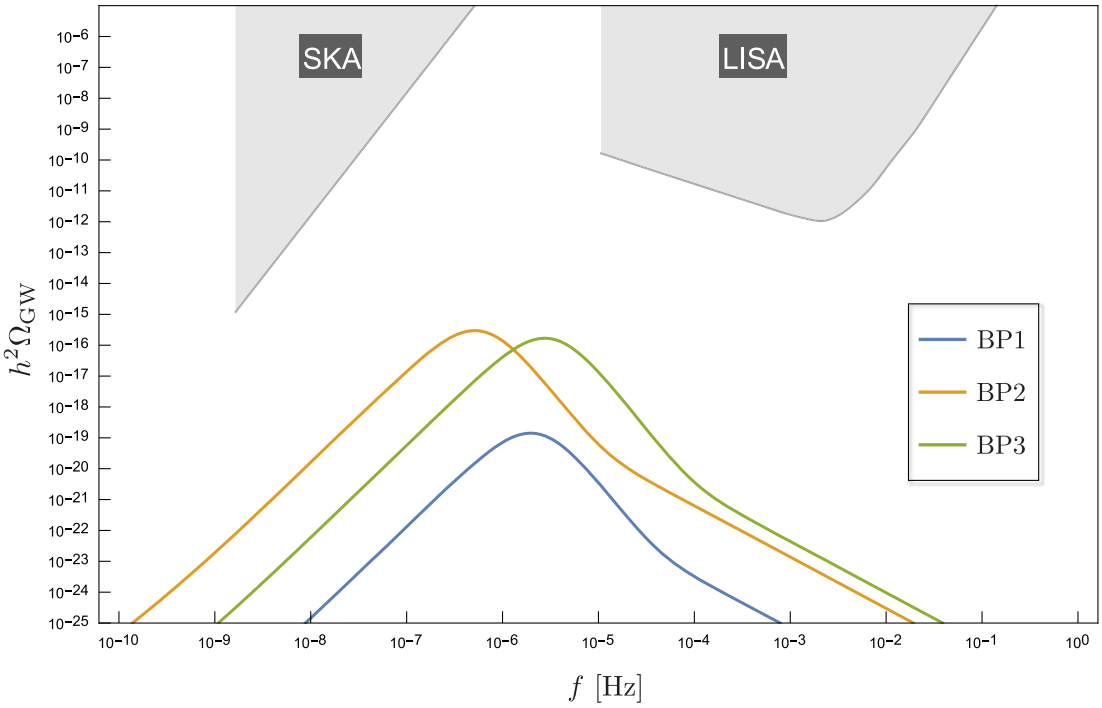

FIG. 6. MeV scale $U(1)'$ phase transition GWs spectrums for three benchmark points. Gray areas are detection regions of SKA and LISA.

$$f_t^{\text{peak}} = 13.0 \times 10^{-11}\ \text{Hz} \left(\frac{g_{\text{eff}*}^{1/2}}{h_{\text{eff}*}^{1/3}}\right)\left(\frac{h_{\text{eff}0}}{3.91}\right)^{1/3} \xi_0 \left(\frac{T_*}{1\ \text{MeV}}\right)\left(\frac{\beta/H_*}{v_w}\right)$$
$$\simeq 4.87 \times 10^{-10}\ \text{Hz} \left(\frac{T_*}{1\ \text{MeV}}\right)\left(\frac{\beta/H_*}{v_w}\right). \quad (80)$$

For our three benchmark points, factor $(\frac{\beta/H_*}{v_w}) \sim \mathcal{O}(1000)$. Thus their peak frequencies are around 10^{-6}–10^{-7} Hz, which is not favored by either SKA telescope [244] or space-based LISA interferometer [245]. In Fig. 6 we present the GWs spectrums of our three benchmark points. As we expected, these signals are not detectable by the SKA or LISA.

However, this result depends significantly on our choice of benchmark point. In order not to change the limit from N_{eff} we got in Sec. III D, for all the benchmark points we consider, the strength of the phase transitions are quite weak (i.e., the value of $\mathbb{A}$ and $\mathbb{A}'$ are quite small). If we increase the intensity of the phase transition and make a strong supercooling, then the generated GWs signal might be detected by SKA. The reason is twofold. First, $h^2\Omega_{\text{GW}}$ is approximately proportional to $\mathbb{A}^2$. So increasing $\mathbb{A}$ by an order of magnitude, we can increase $h^2\Omega_{\text{GW}}$ by roughly 2 orders of magnitude. Second, strong supercooling will decrease the value of factor β/H_* and thus make the peak frequency of $h^2\Omega_{\text{GW}}$ closer to the detection region of SKA. But due to the vast entropy released in the strong supercooling case, the generated DM asymmetry will be diluted and N_{eff} will be enhanced. So the strong supercooling case requires a more detailed analysis. We leave it for a future study.

VI. CONCLUSION

In this work we propose an asymmetry DM model with massive mediator to explain DM small scale structure data and to avoid the limit from CMB. In our model, the DM candidate is a vectorlike fermion charged under a dark $U(1)'$, and the mediator is the $U(1)'$ gauge boson that gain mass from the spontaneous symmetry breaking. The asymmetry between DM and anti-DM is generated by the CP violated and out-of-equilibrium decay of a neutral heavy fermion. The model is consistent with cosmology observations like CMB and LLS. The existence of dark radiation increases the value of N_{eff}, and it makes this model detectable by the future measurement of N_{eff}. Finally, the MeV scale $U(1)'$ symmetry breaking generates GWs signal with peak frequency around 10^{-6}–10^{-7} Hz. It also possible to make the GWs from $U(1)'$ symmetry breaking to be detected by SKA, if we consider a strong supercooling phase transition.

ACKNOWLEDGMENTS

M. Z. thanks Song Li and Yang Xiao for useful discussions. This work was supported by the National Natural Science Foundation of China (NNSFC) under Grants No. 12105118 and No. 11947118.

[1] P. A. R. Ade *et al.* (Planck Collaboration), Planck 2015 results. XIII. Cosmological parameters, Astron. Astrophys. **594**, A13 (2016).
[2] D. Clowe, M. Bradac, A. H. Gonzalez, M. Markevitch, S. W. Randall, C. Jones, and D. Zaritsky, A direct empirical proof of the existence of dark matter, Astrophys. J. Lett. **648**, L109 (2006).
[3] G. R. Blumenthal, S. M. Faber, J. R. Primack, and M. J. Rees, Formation of galaxies and large scale structure with cold dark matter, Nature (London) **311**, 517 (1984).
[4] V. Springel, C. S. Frenk, and S. D. M. White, The large-scale structure of the Universe, Nature (London) **440**, 1137 (2006).
[5] R. A. Flores and J. R. Primack, Observational and theoretical constraints on singular dark matter halos, Astrophys. J. Lett. **427**, L1 (1994).
[6] B. Moore, Evidence against dissipationless dark matter from observations of galaxy haloes, Nature (London) **370**, 629 (1994).
[7] B. Moore, T. R. Quinn, F. Governato, J. Stadel, and G. Lake, Cold collapse and the core catastrophe, Mon. Not. R. Astron. Soc. **310**, 1147 (1999).
[8] K. A. Oman, J. F. Navarro, A. Fattahi, C. S. Frenk, T. Sawala, S. D. M. White, R. Bower, R. A. Crain, M. Furlong, M. Schaller *et al.*, The unexpected diversity of dwarf galaxy rotation curves, Mon. Not. R. Astron. Soc. **452**, 3650 (2015).

[9] A. A. Klypin, A. V. Kravtsov, O. Valenzuela, and F. Prada, Where are the missing Galactic satellites?, Astrophys. J. **522**, 82 (1999).
[10] B. Moore, S. Ghigna, F. Governato, G. Lake, T. R. Quinn, J. Stadel, and P. Tozzi, Dark matter substructure within galactic halos, Astrophys. J. Lett. **524**, L19 (1999).
[11] M. Boylan-Kolchin, J. S. Bullock, and M. Kaplinghat, Too big to fail? The puzzling darkness of massive Milky Way subhaloes, Mon. Not. R. Astron. Soc. **415**, L40 (2011).
[12] M. Boylan-Kolchin, J. S. Bullock, and M. Kaplinghat, The Milky Way's bright satellites as an apparent failure of LCDM, Mon. Not. R. Astron. Soc. **422**, 1203 (2012).
[13] J. F. Navarro, V. R. Eke, and C. S. Frenk, The cores of dwarf galaxy halos, Mon. Not. R. Astron. Soc. **283**, L72 (1996).
[14] F. Governato, C. Brook, L. Mayer, A. Brooks, G. Rhee, J. Wadsley, P. Jonsson, B. Willman, G. Stinson, T. Quinn *et al.*, At the heart of the matter: The origin of bulgeless dwarf galaxies and Dark Matter cores, Nature (London) **463**, 203 (2010).
[15] D. N. Spergel and P. J. Steinhardt, Observational Evidence for Selfinteracting Cold Dark Matter, Phys. Rev. Lett. **84**, 3760 (2000).
[16] M. Rocha, A. H. G. Peter, J. S. Bullock, M. Kaplinghat, S. Garrison-Kimmel, J. Onorbe, and L. A. Moustakas, Cosmological simulations with self-interacting dark matter I: Constant density cores and substructure, Mon. Not. R. Astron. Soc. **430**, 81 (2013).
[17] A. H. G. Peter, M. Rocha, J. S. Bullock, and M. Kaplinghat, Cosmological simulations with self-interacting dark matter II: Halo shapes vs. observations, Mon. Not. R. Astron. Soc. **430**, 105 (2013).
[18] B. Moore, S. Gelato, A. Jenkins, F. R. Pearce, and V. Quilis, Collisional versus collisionless dark matter, Astrophys. J. Lett. **535**, L21 (2000).
[19] N. Yoshida, V. Springel, S. D. M. White, and G. Tormen, Collisional dark matter and the structure of dark halos, Astrophys. J. Lett. **535**, L103 (2000).
[20] A. Burkert, The structure and evolution of weakly self-interacting cold dark matter halos, Astrophys. J. Lett. **534**, L143 (2000).
[21] C. S. Kochanek and M. J. White, A quantitative study of interacting dark matter in halos, Astrophys. J. **543**, 514 (2000).
[22] N. Yoshida, V. Springel, S. D. M. White, and G. Tormen, Weakly self-interacting dark matter and the structure of dark halos, Astrophys. J. Lett. **544**, L87 (2000).
[23] R. Dave, D. N. Spergel, P. J. Steinhardt, and B. D. Wandelt, Halo properties in cosmological simulations of self-interacting cold dark matter, Astrophys. J. **547**, 574 (2001).
[24] P. Colin, V. Avila-Reese, O. Valenzuela, and C. Firmani, Structure and subhalo population of halos in a self-interacting dark matter cosmology, Astrophys. J. **581**, 777 (2002).
[25] M. Vogelsberger, J. Zavala, and A. Loeb, Subhaloes in self-interacting galactic dark matter haloes, Mon. Not. R. Astron. Soc. **423**, 3740 (2012).
[26] J. Zavala, M. Vogelsberger, and M. G. Walker, Constraining self-interacting dark matter with the Milky Way's dwarf spheroidals, Mon. Not. R. Astron. Soc. **431**, L20 (2013).
[27] O. D. Elbert, J. S. Bullock, S. Garrison-Kimmel, M. Rocha, J. Oñorbe, and A. H. G. Peter, Core formation in dwarf haloes with self-interacting dark matter: No fine-tuning necessary, Mon. Not. R. Astron. Soc. **453**, 29 (2015).
[28] M. Vogelsberger, J. Zavala, C. Simpson, and A. Jenkins, Dwarf galaxies in CDM and SIDM with baryons: Observational probes of the nature of dark matter, Mon. Not. R. Astron. Soc. **444**, 3684 (2014).
[29] A. B. Fry, F. Governato, A. Pontzen, T. Quinn, M. Tremmel, L. Anderson, H. Menon, A. M. Brooks, and J. Wadsley, All about baryons: Revisiting SIDM predictions at small halo masses, Mon. Not. R. Astron. Soc. **452**, 1468 (2015).
[30] G. A. Dooley, A. H. G. Peter, M. Vogelsberger, J. Zavala, and A. Frebel, Enhanced tidal stripping of satellites in the galactic halo from dark matter self-interactions, Mon. Not. R. Astron. Soc. **461**, 710 (2016).
[31] D. Harvey, R. Massey, T. Kitching, A. Taylor, and E. Tittley, The non-gravitational interactions of dark matter in colliding galaxy clusters, Science **347**, 1462 (2015).
[32] M. Kaplinghat, S. Tulin, and H. B. Yu, Dark Matter Halos as Particle Colliders: Unified Solution to Small-Scale Structure Puzzles from Dwarfs to Clusters, Phys. Rev. Lett. **116**, 041302 (2016).
[33] A. Robertson, D. Harvey, R. Massey, V. Eke, I. G. McCarthy, M. Jauzac, B. Li, and J. Schaye, Observable tests of self-interacting dark matter in galaxy clusters: Cosmological simulations with SIDM and baryons, Mon. Not. R. Astron. Soc. **488**, 3646 (2019).
[34] L. Sagunski, S. Gad-Nasr, B. Colquhoun, A. Robertson, and S. Tulin, Velocity-dependent Self-interacting dark matter from groups and clusters of galaxies, J. Cosmol. Astropart. Phys. 01 (2021) 024.
[35] K. E. Andrade, J. Fuson, S. Gad-Nasr, D. Kong, Q. Minor, M. G. Roberts, and M. Kaplinghat, A stringent upper limit on dark matter self-interaction cross-section from cluster strong lensing, Mon. Not. R. Astron. Soc. **510**, 54 (2021).
[36] O. D. Elbert, J. S. Bullock, M. Kaplinghat, S. Garrison-Kimmel, A. S. Graus, and M. Rocha, A testable conspiracy: Simulating baryonic effects on self-interacting dark matter halos, Astrophys. J. **853**, 109 (2018).
[37] S. Tulin and H. B. Yu, Dark matter self-interactions and small scale structure, Phys. Rep. **730**, 1 (2018).
[38] M. R. Buckley and P. J. Fox, Dark matter self-interactions and light force carriers, Phys. Rev. D **81**, 083522 (2010).
[39] J. L. Feng, M. Kaplinghat, and H. B. Yu, Halo Shape and Relic Density Exclusions of Sommerfeld-Enhanced Dark Matter Explanations of Cosmic Ray Excesses, Phys. Rev. Lett. **104**, 151301 (2010).
[40] J. L. Feng, M. Kaplinghat, H. Tu, and H. B. Yu, Hidden charged dark matter, J. Cosmol. Astropart. Phys. 07 (2009) 004.
[41] A. Loeb and N. Weiner, Cores in Dwarf Galaxies from Dark Matter with a Yukawa Potential, Phys. Rev. Lett. **106**, 171302 (2011).
[42] L. G. van den Aarssen, T. Bringmann, and C. Pfrommer, Is Dark Matter with Long-Range Interactions a Solution to

All Small-Scale Problems of Λ CDM Cosmology?, Phys. Rev. Lett. **109**, 231301 (2012).
[43] S. Tulin, H. B. Yu, and K. M. Zurek, Beyond collisionless dark matter: Particle physics dynamics for dark matter halo structure, Phys. Rev. D **87**, 115007 (2013).
[44] K. Schutz and T. R. Slatyer, Self-scattering for dark matter with an excited state, J. Cosmol. Astropart. Phys. 01 (2015) 021.
[45] S. Tulin, H. B. Yu, and K. M. Zurek, Resonant Dark Forces and Small Scale Structure, Phys. Rev. Lett. **110**, 111301 (2013).
[46] K. K. Boddy, J. L. Feng, M. Kaplinghat, Y. Shadmi, and T. M. P. Tait, Strongly interacting dark matter: Self-interactions and keV lines, Phys. Rev. D **90**, 095016 (2014).
[47] P. Ko and Y. Tang, Self-interacting scalar dark matter with local Z_3 symmetry, J. Cosmol. Astropart. Phys. 05 (2014) 047.
[48] Z. Kang, View FImP miracle (by scale invariance) *à la* self-interaction, Phys. Lett. B **751**, 201 (2015).
[49] K. Kainulainen, K. Tuominen, and V. Vaskonen, Self-interacting dark matter and cosmology of a light scalar mediator, Phys. Rev. D **93**, 015016 (2016); **95**, 079901(E) (2017).
[50] W. Wang, M. Zhang, and J. Zhao, Higgs exotic decays in general NMSSM with self-interacting dark matter, Int. J. Mod. Phys. A **33**, 1841002 (2018).
[51] M. Duerr, K. Schmidt-Hoberg, and S. Wild, Self-interacting dark matter with a stable vector mediator, J. Cosmol. Astropart. Phys. 09 (2018) 033.
[52] T. Kitahara and Y. Yamamoto, Protophobic light vector boson as a mediator to the dark sector, Phys. Rev. D **95**, 015008 (2017).
[53] E. Ma, Inception of self-interacting dark matter with dark charge conjugation symmetry, Phys. Lett. B **772**, 442 (2017).
[54] B. Bellazzini, M. Cliche, and P. Tanedo, Effective theory of self-interacting dark matter, Phys. Rev. D **88**, 083506 (2013).
[55] A. Kamada, H. J. Kim, and T. Kuwahara, Maximally self-interacting dark matter: Models and predictions, J. High Energy Phys. 12 (2020) 202.
[56] A. Kamada, M. Yamada, and T. T. Yanagida, Unification for darkly charged dark matter, Phys. Rev. D **102**, 015012 (2020).
[57] A. Kamada, M. Yamada, and T. T. Yanagida, Unification of the standard model and dark matter sectors in $[\mathrm{SU}(5)\times\mathrm{U}(1)]^4$, J. High Energy Phys. 07 (2019) 180.
[58] T. Bringmann, J. Hasenkamp, and J. Kersten, Tight bonds between sterile neutrinos and dark matter, J. Cosmol. Astropart. Phys. 07 (2014) 042.
[59] P. Ko and Y. Tang, $\nu\Lambda$MDM: A model for sterile neutrino and dark matter reconciles cosmological and neutrino oscillation data after BICEP2, Phys. Lett. B **739**, 62 (2014).
[60] A. Kamada, K. Kaneta, K. Yanagi, and H. B. Yu, Self-interacting dark matter and muon $g-2$ in a gauged $\mathrm{U}(1)_{L_\mu-L_\tau}$ model, J. High Energy Phys. 06 (2018) 117.
[61] A. Kamada, M. Yamada, and T. T. Yanagida, Self-interacting dark matter with a vector mediator: Kinetic mixing with the $\mathrm{U}(1)_{(B-L)_3}$ gauge boson, J. High Energy Phys. 03 (2019) 021.
[62] A. Aboubrahim, W. Z. Feng, P. Nath, and Z. Y. Wang, Self-interacting hidden sector dark matter, small scale galaxy structure anomalies, and a dark force, Phys. Rev. D **103**, 075014 (2021).
[63] R. Foot and S. Vagnozzi, Dissipative hidden sector dark matter, Phys. Rev. D **91**, 023512 (2015).
[64] R. Foot and S. Vagnozzi, Diurnal modulation signal from dissipative hidden sector dark matter, Phys. Lett. B **748**, 61 (2015).
[65] R. Foot and S. Vagnozzi, Solving the small-scale structure puzzles with dissipative dark matter, J. Cosmol. Astropart. Phys. 07 (2016) 013.
[66] M. Pospelov, A. Ritz, and M. B. Voloshin, Secluded WIMP dark matter, Phys. Lett. B **662**, 53 (2008).
[67] A. Tan *et al.* (PandaX-II Collaboration), Dark Matter Results from First 98.7 Days of Data from the PandaX-II Experiment, Phys. Rev. Lett. **117**, 121303 (2016).
[68] D. S. Akerib *et al.* (LUX Collaboration), Results from a Search for Dark Matter in the Complete LUX Exposure, Phys. Rev. Lett. **118**, 021303 (2017).
[69] V. Khachatryan *et al.* (CMS Collaboration), Search for dark matter particles in proton-proton collisions at $\sqrt{s}=$ 8 TeV using the razor variables, J. High Energy Phys. 12 (2016) 088.
[70] G. Aad *et al.* (ATLAS Collaboration), Search for Dark Matter in Events with a Hadronically Decaying W or Z Boson and Missing Transverse Momentum in pp Collisions at $\sqrt{s}=8$ TeV with the ATLAS Detector, Phys. Rev. Lett. **112**, 041802 (2014).
[71] D. Abercrombie *et al.*, Dark matter benchmark models for early LHC Run-2 searches: Report of the ATLAS/CMS dark matter forum, Phys. Dark Universe **27**, 100371 (2020).
[72] M. Aaboud *et al.* (ATLAS Collaboration), Search for dark matter at $\sqrt{s}=13$ TeV in final states containing an energetic photon and large missing transverse momentum with the ATLAS detector, Eur. Phys. J. C **77**, 393 (2017).
[73] M. Aaboud *et al.* (ATLAS Collaboration), Search for Dark Matter Produced in Association with a Higgs Boson Decaying to $b\bar{b}$ using 36 fb^{-1} of pp Collisions at $\sqrt{s}=$ 13 TeV with the ATLAS Detector, Phys. Rev. Lett. **119**, 181804 (2017).
[74] M. Kamionkowski and S. Profumo, Early Annihilation and Diffuse Backgrounds in Models of Weakly Interacting Massive Particles in Which the Cross Section for Pair Annihilation is Enhanced by $1/v$, Phys. Rev. Lett. **101**, 261301 (2008).
[75] J. Zavala, M. Vogelsberger, and S. D. M. White, Relic density and CMB constraints on dark matter annihilation with Sommerfeld enhancement, Phys. Rev. D **81**, 083502 (2010).
[76] J. L. Feng, M. Kaplinghat, and H. B. Yu, Sommerfeld enhancements for thermal relic dark matter, Phys. Rev. D **82**, 083525 (2010).
[77] J. Hisano, M. Kawasaki, K. Kohri, T. Moroi, K. Nakayama, and T. Sekiguchi, Cosmological constraints on dark matter models with velocity-dependent annihilation cross section, Phys. Rev. D **83**, 123511 (2011).

[78] L. Bergström, G. Bertone, T. Bringmann, J. Edsjö, and M. Taoso, Gamma-ray and radio constraints of high positron rate dark matter models annihilating into new light particles, Phys. Rev. D **79**, 081303 (2009).
[79] J. Mardon, Y. Nomura, D. Stolarski, and J. Thaler, Dark matter signals from cascade annihilations, J. Cosmol. Astropart. Phys. 05 (2009) 016.
[80] S. Hannestad and T. Tram, Sommerfeld enhancement of DM annihilation: Resonance structure, freeze-out and CMB spectral bound, J. Cosmol. Astropart. Phys. 01 (2011) 016.
[81] D. P. Finkbeiner, L. Goodenough, T. R. Slatyer, M. Vogelsberger, and N. Weiner, Consistent scenarios for cosmic-ray excesses from Sommerfeld-enhanced dark matter annihilation, J. Cosmol. Astropart. Phys. 05 (2011) 002.
[82] S. Galli, F. Iocco, G. Bertone, and A. Melchiorri, CMB constraints on dark matter models with large annihilation cross-section, Phys. Rev. D **80**, 023505 (2009).
[83] T. R. Slatyer, N. Padmanabhan, and D. P. Finkbeiner, CMB constraints on WIMP annihilation: Energy absorption during the recombination epoch, Phys. Rev. D **80**, 043526 (2009).
[84] A. Sommerfeld, Über die Beugung und Bremsung der Elektronen Ann. Phys. (Berlin) **403**, 257 (1931).
[85] J. Hisano, S. Matsumoto, and M. M. Nojiri, Explosive Dark Matter Annihilation, Phys. Rev. Lett. **92**, 031303 (2004).
[86] J. Hisano, S. Matsumoto, M. M. Nojiri, and O. Saito, Non-perturbative effect on dark matter annihilation and gamma ray signature from galactic center, Phys. Rev. D **71**, 063528 (2005).
[87] J. Hisano, S. Matsumoto, O. Saito, and M. Senami, Heavy wino-like neutralino dark matter annihilation into anti-particles, Phys. Rev. D **73**, 055004 (2006).
[88] M. Cirelli, A. Strumia, and M. Tamburini, Cosmology and astrophysics of minimal dark matter, Nucl. Phys. **B787**, 152 (2007).
[89] N. Arkani-Hamed, D. P. Finkbeiner, T. R. Slatyer, and N. Weiner, A theory of dark matter, Phys. Rev. D **79**, 015014 (2009).
[90] I. Cholis, D. P. Finkbeiner, L. Goodenough, and N. Weiner, The PAMELA positron excess from annihilations into a light boson, J. Cosmol. Astropart. Phys. 12 (2009) 007.
[91] T. Bringmann, F. Kahlhoefer, K. Schmidt-Hoberg, and P. Walia, Strong Constraints on Self-Interacting Dark Matter with Light Mediators, Phys. Rev. Lett. **118**, 141802 (2017).
[92] D. E. Kaplan, M. A. Luty, and K. M. Zurek, Asymmetric dark matter, Phys. Rev. D **79**, 115016 (2009).
[93] K. Petraki and R. R. Volkas, Review of asymmetric dark matter, Int. J. Mod. Phys. A **28**, 1330028 (2013).
[94] K. M. Zurek, Asymmetric dark matter: Theories, signatures, and constraints, Phys. Rept. **537**, 91 (2014).
[95] T. Lin, H. B. Yu, and K. M. Zurek, On symmetric and asymmetric light dark matter, Phys. Rev. D **85**, 063503 (2012).
[96] I. Baldes, M. Cirelli, P. Panci, K. Petraki, F. Sala, and M. Taoso, Asymmetric dark matter: Residual annihilations and self-interactions, SciPost Phys. **4**, 041 (2018).
[97] S. Nussinov, Technocosmology: Could a technibaryon excess provide a 'natural' missing mass candidate?, Phys. Lett. **165B**, 55 (1985).
[98] D. B. Kaplan, A Single Explanation for Both the Baryon and Dark Matter Densities, Phys. Rev. Lett. **68**, 741 (1992).
[99] S. M. Barr, R. S. Chivukula, and E. Farhi, Electroweak fermion number violation and the production of stable particles in the early universe, Phys. Lett. B **241**, 387 (1990).
[100] S. M. Barr, Baryogenesis, sphalerons and the cogeneration of dark matter, Phys. Rev. D **44**, 3062 (1991).
[101] S. Dodelson, B. R. Greene, and L. M. Widrow, Baryogenesis, dark matter and the width of the Z, Nucl. Phys. **B372**, 467 (1992).
[102] M. Fujii and T. Yanagida, A solution to the coincidence puzzle of Omega(B) and Omega (DM), Phys. Lett. B **542**, 80 (2002).
[103] R. Kitano and I. Low, Dark matter from baryon asymmetry, Phys. Rev. D **71**, 023510 (2005).
[104] G. R. Farrar and G. Zaharijas, Dark Matter and the Baryon Asymmetry, Phys. Rev. Lett. **96**, 041302 (2006).
[105] R. Kitano, H. Murayama, and M. Ratz, Unified origin of baryons and dark matter, Phys. Lett. B **669**, 145 (2008).
[106] S. B. Gudnason, C. Kouvaris, and F. Sannino, Towards working technicolor: Effective theories and dark matter, Phys. Rev. D **73**, 115003 (2006).
[107] J. Shelton and K. M. Zurek, Darkogenesis: A baryon asymmetry from the dark matter sector, Phys. Rev. D **82**, 123512 (2010).
[108] H. Davoudiasl, D. E. Morrissey, K. Sigurdson, and S. Tulin, Hylogenesis: A Unified Origin for Baryonic Visible Matter and Antibaryonic Dark Matter, Phys. Rev. Lett. **105**, 211304 (2010).
[109] F. P. Huang and C. S. Li, Probing the baryogenesis and dark matter relaxed in phase transition by gravitational waves and colliders, Phys. Rev. D **96**, 095028 (2017).
[110] M. R. Buckley and L. Randall, Xogenesis, J. High Energy Phys. 09 (2011) 009.
[111] T. Cohen, D. J. Phalen, A. Pierce, and K. M. Zurek, Asymmetric dark matter from a GeV hidden sector, Phys. Rev. D **82**, 056001 (2010).
[112] M. Ibe, A. Kamada, S. Kobayashi, and W. Nakano, Composite asymmetric dark matter with a dark photon portal, J. High Energy Phys. 11 (2018) 203.
[113] M. Ibe, A. Kamada, S. Kobayashi, T. Kuwahara, and W. Nakano, Ultraviolet completion of a composite asymmetric dark matter model with a dark photon portal, J. High Energy Phys. 03 (2019) 173.
[114] H. An, S. L. Chen, R. N. Mohapatra, and Y. Zhang, Leptogenesis as a common origin for matter and dark matter, J. High Energy Phys. 03 (2010) 124.
[115] A. Falkowski, J. T. Ruderman, and T. Volansky, Asymmetric dark matter from leptogenesis, J. High Energy Phys. 05 (2011) 106.
[116] Y. Bai and P. Schwaller, Scale of dark QCD, Phys. Rev. D **89**, 063522 (2014).
[117] M. Zhang, Leptophilic composite asymmetric dark matter and its detection, Phys. Rev. D **104**, 055008 (2021).

[118] D. S. M. Alves, S. R. Behbahani, P. Schuster, and J. G. Wacker, Composite inelastic dark matter, Phys. Lett. B **692**, 323 (2010).

[119] D. Spier Moreira Alves, S. R. Behbahani, P. Schuster, and J. G. Wacker, The cosmology of composite inelastic dark matter, J. High Energy Phys. 06 (2010) 113.

[120] V. Beylin, M. Khlopov, V. Kuksa, and N. Volchanskiy, New physics of strong interaction and dark universe, Universe **6**, 196 (2020).

[121] M. Y. Khlopov, G. M. Beskin, N. E. Bochkarev, L. A. Pustylnik, and S. A. Pustylnik, Observational physics of mirror world, Sov. Astron. **35**, 21 (1991).

[122] S. I. Blinnikov and M. Khlopov, Possible astronomical effects of mirror particles, Sov. Astron. **27**, 371 (1983).

[123] S. I. Blinnikov and M. Y. Khlopov, On possible effects of "mirror" particles, Sov. J. Nucl. Phys. **36**, 472 (1982).

[124] M. Blennow, E. Fernandez-Martinez, O. Mena, J. Redondo, and P. Serra, Asymmetric dark matter and dark radiation, J. Cosmol. Astropart. Phys. 07 (2012) 022.

[125] M. T. Frandsen, S. Sarkar, and K. Schmidt-Hoberg, Light asymmetric dark matter from new strong dynamics, Phys. Rev. D **84**, 051703 (2011).

[126] C. Murgui and K. M. Zurek, Dark Unification: A UV-complete theory of asymmetric dark matter, Phys. Rev. D **105**, 095002 (2022).

[127] A. Kamada and T. Kuwahara, LHC lifetime frontier and visible decay searches in composite asymmetric dark matter models, J. High Energy Phys. 03 (2022) 176.

[128] M. Ibe, A. Kamada, S. Kobayashi, T. Kuwahara, and W. Nakano, Baryon-dark matter coincidence in mirrored unification, Phys. Rev. D **100**, 075022 (2019).

[129] R. N. Mohapatra, S. Nussinov, and V. L. Teplitz, Mirror matter as selfinteracting dark matter, Phys. Rev. D **66**, 063002 (2002).

[130] M. T. Frandsen and S. Sarkar, Asymmetric Dark Matter and the Sun, Phys. Rev. Lett. **105**, 011301 (2010).

[131] K. Petraki, L. Pearce, and A. Kusenko, Self-interacting asymmetric dark matter coupled to a light massive dark photon, J. Cosmol. Astropart. Phys. 07 (2014) 039.

[132] C. Dessert, C. Kilic, C. Trendafilova, and Y. Tsai, Addressing astrophysical and cosmological problems with secretly asymmetric dark matter, Phys. Rev. D **100**, 015029 (2019).

[133] M. Dutta, N. Narendra, N. Sahu, and S. Shil, Asymmetric self-interacting dark matter via dirac leptogenesis, Phys. Rev. D **106**, 095017 (2022).

[134] J. Heeck and A. Thapa, Explaining lepton-flavor non-universality and self-interacting dark matter with $L_\mu - L_\tau$, Eur. Phys. J. C **82**, 480 (2022).

[135] E. Hall, T. Konstandin, R. McGehee, and H. Murayama, Asymmetric matter from a dark first-order phase transition, Phys. Rev. D **107**, 055011 (2023).

[136] E. Hall, R. McGehee, H. Murayama, and B. Suter, Asymmetric dark matter may not be light, Phys. Rev. D **106**, 075008 (2022).

[137] Y. D. Tsai, R. McGehee, and H. Murayama, Resonant Self-Interacting Dark Matter from Dark QCD, Phys. Rev. Lett. **128**, 17 (2022).

[138] P. F. Perez, C. Murgui, and A. D. Plascencia, Baryogenesis via leptogenesis: Spontaneous B and L violation, Phys. Rev. D **104**, 055007 (2021).

[139] M. R. Buckley and S. Profumo, Regenerating a Symmetry in Asymmetric Dark Matter, Phys. Rev. Lett. **108**, 011301 (2012).

[140] S. Tulin, H. B. Yu, and K. M. Zurek, Oscillating asymmetric dark matter, J. Cosmol. Astropart. Phys. 05 (2012) 013.

[141] L. Husdal, On effective degrees of freedom in the early universe, Galaxies **4**, 78 (2016).

[142] M. Fukugita and T. Yanagida, Baryogenesis without grand unification, Phys. Lett. B **174**, 45 (1986).

[143] W. Buchmuller, P. Di Bari, and M. Plumacher, Leptogenesis for pedestrians, Ann. Phys. (Amsterdam) **315**, 305 (2005).

[144] S. Davidson, E. Nardi, and Y. Nir, Leptogenesis, Phys. Rep. **466**, 105 (2008).

[145] L. Covi, E. Roulet, and F. Vissani, *CP* violating decays in leptogenesis scenarios, Phys. Lett. B **384**, 169 (1996).

[146] R. J. Scherrer and M. S. Turner, On the Relic, Cosmic abundance of stable weakly interacting massive particles, Phys. Rev. D **33**, 1585 (1986); **34**, 3263(E) (1986).

[147] K. Griest and D. Seckel, Cosmic asymmetry, neutrinos and the sun, Nucl. Phys. **B283**, 681 (1987); **B296**, 1034(E) (1988).

[148] M. L. Graesser, I. M. Shoemaker, and L. Vecchi, Asymmetric WIMP dark matter, J. High Energy Phys. 10 (2011) 110.

[149] H. Iminniyaz, M. Drees, and X. Chen, Relic abundance of asymmetric dark matter, J. Cosmol. Astropart. Phys. 07 (2011) 003.

[150] N. F. Bell, S. Horiuchi, and I. M. Shoemaker, Annihilating asymmetric dark matter, Phys. Rev. D **91**, 023505 (2015).

[151] K. Murase and I. M. Shoemaker, Detecting asymmetric dark matter in the sun with neutrinos, Phys. Rev. D **94**, 063512 (2016).

[152] I. Baldes and K. Petraki, Asymmetric thermal-relic dark matter: Sommerfeld-enhanced freeze-out, annihilation signals and unitarity bounds, J. Cosmol. Astropart. Phys. 09 (2017) 028.

[153] M. Hufnagel, K. Schmidt-Hoberg, and S. Wild, BBN constraints on MeV-scale dark sectors. Part II. Electromagnetic decays, J. Cosmol. Astropart. Phys. 11 (2018) 032.

[154] P. F. Depta, M. Hufnagel, and K. Schmidt-Hoberg, Updated BBN constraints on electromagnetic decays of MeV-scale particles, J. Cosmol. Astropart. Phys. 04 (2021) 011.

[155] M. Ibe, S. Kobayashi, Y. Nakayama, and S. Shirai, Cosmological constraints on dark scalar, J. High Energy Phys. 03 (2022) 198.

[156] J. H. Chang, R. Essig, and S. D. McDermott, Revisiting supernova 1987A constraints on dark photons, J. High Energy Phys. 01 (2017) 107.

[157] E. Del Nobile, M. Kaplinghat, and H. B. Yu, Direct detection signatures of self-interacting dark matter with a light mediator, J. Cosmol. Astropart. Phys. 10 (2015) 055.

[158] S. Cassel, Sommerfeld factor for arbitrary partial wave processes, J. Phys. G **37**, 105009 (2010).

[159] J. M. Cline and P. Scott, Dark matter CMB constraints and likelihoods for poor particle physicists, J. Cosmol. Astropart. Phys. 03 (2013) 044; 05 (2013) E01.

[160] H. Liu, T. R. Slatyer, and J. Zavala, Contributions to cosmic reionization from dark matter annihilation and decay, Phys. Rev. D **94**, 063507 (2016).

[161] M. Kawasaki, H. Nakatsuka, K. Nakayama, and T. Sekiguchi, Revisiting CMB constraints on dark matter annihilation, J. Cosmol. Astropart. Phys. 12 (2021) 015.
[162] N. Aghanim *et al.* (Planck Collabroation), Planck 2018 results. V. CMB power spectra and likelihoods, Astron. Astrophys. **641**, A5 (2020).
[163] L. Anderson *et al.* (BOSS Collaboration), The clustering of galaxies in the SDSS-III Baryon Oscillation Spectroscopic Survey: Baryon acoustic oscillations in the Data Releases 10 and 11 Galaxy samples, Mon. Not. R. Astron. Soc. **441**, 24 (2014).
[164] A. J. Ross, L. Samushia, C. Howlett, W. J. Percival, A. Burden, and M. Manera, The clustering of the SDSS DR7 main Galaxy sample—I. A 4 per cent distance measure at $z = 0.15$, Mon. Not. R. Astron. Soc. **449**, 835 (2015).
[165] T. M. C. Abbott *et al.* (DES Collaboration), Dark energy survey year 1 results: Cosmological constraints from galaxy clustering and weak lensing, Phys. Rev. D **98**, 043526 (2018).
[166] N. Aghanim *et al.* (Planck Collaboration), Planck 2018 results. VI. Cosmological parameters, Astron. Astrophys. **641**, A6 (2020); **652**, C4(E) (2021).
[167] P. F. de Salas and S. Pastor, Relic neutrino decoupling with flavour oscillations revisited, J. Cosmol. Astropart. Phys. 07 (2016) 051.
[168] Y. Bai and M. Korwar, Cosmological constraints on first-order phase transitions, Phys. Rev. D **105**, 095015 (2022).
[169] K. Abazajian *et al.* (CMB-S4 Collaboration), Snowmass 2021 CMB-S4 white paper, arXiv:2203.08024.
[170] F. Y. Cyr-Racine, R. de Putter, A. Raccanelli, and K. Sigurdson, Constraints on large-scale dark acoustic oscillations from cosmology, Phys. Rev. D **89**, 063517 (2014).
[171] M. R. Buckley, J. Zavala, F. Y. Cyr-Racine, K. Sigurdson, and M. Vogelsberger, Scattering, damping, and acoustic oscillations: Simulating the structure of dark matter halos with relativistic force carriers, Phys. Rev. D **90**, 043524 (2014).
[172] F. Kahlhoefer, K. Schmidt-Hoberg, and S. Wild, Dark matter self-interactions from a general spin-0 mediator, J. Cosmol. Astropart. Phys. 08 (**2017**) 003.
[173] S. A. Khrapak, A. V. Ivlev, G. E. Morfill, and S. K. Zhdanov, Scattering in the Attractive Yukawa Potential in the Limit of Strong Interaction, Phys. Rev. Lett. **90**, 225002 (2003).
[174] F. Y. Cyr-Racine, K. Sigurdson, J. Zavala, T. Bringmann, M. Vogelsberger, and C. Pfrommer, ETHOS—an effective theory of structure formation: From dark particle physics to the matter distribution of the Universe, Phys. Rev. D **93**, 123527 (2016).
[175] B. Colquhoun, S. Heeba, F. Kahlhoefer, L. Sagunski, and S. Tulin, Semiclassical regime for dark matter self-interactions, Phys. Rev. D **103**, 035006 (2021).
[176] W. G. Vincenti and C. H. Kruger, *Introduction to Physical Gas Dynamics* (Krieger, Malabar, FL, 1965).
[177] E. Witten, Cosmic separation of phases, Phys. Rev. D **30**, 272 (1984).
[178] J. Jaeckel, V. V. Khoze, and M. Spannowsky, Hearing the signal of dark sectors with gravitational wave detectors, Phys. Rev. D **94**, 103519 (2016).
[179] P. Schwaller, Gravitational Waves from a Dark Phase Transition, Phys. Rev. Lett. **115**, 181101 (2015).
[180] A. Soni and Y. Zhang, Gravitational waves from SU(N) glueball dark matter, Phys. Lett. B **771**, 379 (2017).
[181] A. Addazi and A. Marciano, Gravitational waves from dark first order phase transitions and dark photons, Chin. Phys. C **42**, 023107 (2018).
[182] K. Tsumura, M. Yamada, and Y. Yamaguchi, Gravitational wave from dark sector with dark pion, J. Cosmol. Astropart. Phys. 07 (2017) 044.
[183] F. P. Huang and J. H. Yu, Exploring inert dark matter blind spots with gravitational wave signatures, Phys. Rev. D **98**, 095022 (2018).
[184] K. Hashino, M. Kakizaki, S. Kanemura, P. Ko, and T. Matsui, Gravitational waves from first order electroweak phase transition in models with the $U(1)_X$ gauge symmetry, J. High Energy Phys. 06 (2018) 088.
[185] Y. Bai, A. J. Long, and S. Lu, Dark quark nuggets, Phys. Rev. D **99**, 055047 (2019).
[186] M. Breitbach, J. Kopp, E. Madge, T. Opferkuch, and P. Schwaller, Dark, cold, and noisy: Constraining secluded hidden sectors with gravitational waves, J. Cosmol. Astropart. Phys. 07 (2019) 007.
[187] M. Fairbairn, E. Hardy, and A. Wickens, Hearing without seeing: Gravitational waves from hot and cold hidden sectors, J. High Energy Phys. 07 (2019) 044.
[188] A. Addazi, Y. F. Cai, Q. Gan, A. Marciano, and K. Zeng, NANOGrav results and dark first order phase transitions, Sci. China Phys. Mech. Astron. **64**, 290411 (2021).
[189] W. Ratzinger and P. Schwaller, Whispers from the dark side: Confronting light new physics with NANOGrav data, SciPost Phys. **10**, 047 (2021).
[190] T. Ghosh, H. K. Guo, T. Han, and H. Liu, Electroweak phase transition with an SU(2) dark sector, J. High Energy Phys. 07 (2021) 045.
[191] J. B. Dent, B. Dutta, S. Ghosh, J. Kumar, and J. Runburg, Sensitivity to dark sector scales from gravitational wave signatures, J. High Energy Phys. 08 (2022) 300.
[192] W. Wang, K. P. Xie, W. L. Xu, and J. M. Yang, Cosmological phase transitions, gravitational waves and self-interacting dark matter in the singlet extension of MSSM, Eur. Phys. J. C **82**, 1120 (2022).
[193] W. Wang, W. L. Xu, and J. M. Yang, A hidden self-interacting dark matter sector with first order cosmological phase transition and gravitational wave, arXiv:2209.11408.
[194] A. Azatov, M. Vanvlasselaer, and W. Yin, Dark matter production from relativistic bubble walls, J. High Energy Phys. 03 (2021) 288.
[195] A. Azatov, G. Barni, S. Chakraborty, M. Vanvlasselaer, and W. Yin, Ultra-relativistic bubbles from the simplest Higgs portal and their cosmological consequences, J. High Energy Phys. 10 (2022) 017.
[196] F. Costa, S. Khan, and J. Kim, A two-component dark matter model and its associated gravitational waves, J. High Energy Phys. 06 (**2022**) 026.
[197] F. Costa, S. Khan, and J. Kim, A two-component vector WIMP—fermion FIMP dark matter model with an extended seesaw mechanism, J. High Energy Phys. 12 (2022) 165.

[198] C. Wainwright, S. Profumo, and M. J. Ramsey-Musolf, Gravity waves from a cosmological phase transition: Gauge artifacts and Daisy resummations, Phys. Rev. D **84**, 023521 (2011).
[199] C. W. Chiang and E. Senaha, On gauge dependence of gravitational waves from a first-order phase transition in classical scale-invariant $U(1)'$ models, Phys. Lett. B **774**, 489 (2017).
[200] M. Karjalainen, M. Laine, and J. Peisa, The order of the phase transition in 3-d U(1) + Higgs theory, Nucl. Phys. B, Proc. Suppl. **53**, 475 (1997).
[201] P. Dimopoulos, K. Farakos, and G. Koutsoumbas, Three-dimensional lattice U(1) gauge Higgs model at low m(H), Eur. Phys. J. C **1**, 711 (1998).
[202] S. R. Coleman and E. J. Weinberg, Radiative corrections as the origin of spontaneous symmetry breaking, Phys. Rev. D **7**, 1888 (1973).
[203] C. Delaunay, C. Grojean, and J. D. Wells, Dynamics of non-renormalizable electroweak symmetry breaking, J. High Energy Phys. 04 (**2008**) 029.
[204] G. W. Anderson and L. J. Hall, The electroweak phase transition and baryogenesis, Phys. Rev. D **45**, 2685 (1992).
[205] L. Dolan and R. Jackiw, Symmetry behavior at finite temperature, Phys. Rev. D **9**, 3320 (1974).
[206] M. Quiros, Finite temperature field theory and phase transitions, arXiv:hep-ph/9901312.
[207] P. B. Arnold and O. Espinosa, The effective potential and first order phase transitions: Beyond leading-order, Phys. Rev. D **47**, 3546 (1993); **50**, 6662(E) (1994).
[208] S. R. Coleman, The fate of the false vacuum. 1. Semiclassical theory, Phys. Rev. D **15**, 2929 (1977); **16**, 1248(E) (1977).
[209] C. G. Callan, Jr. and S. R. Coleman, The fate of the false vacuum. 2. First quantum corrections, Phys. Rev. D **16**, 1762 (1977).
[210] A. D. Linde, Decay of the false vacuum at finite temperature, Nucl. Phys. **B216**, 421 (1983); **B223**, 544(E) (1983).
[211] R. Apreda, M. Maggiore, A. Nicolis, and A. Riotto, Gravitational waves from electroweak phase transitions, Nucl. Phys. **B631**, 342 (2002).
[212] C. L. Wainwright, CosmoTransitions: Computing cosmological phase transition temperatures and bubble profiles with multiple fields, Comput. Phys. Commun. **183**, 2006 (2012).
[213] A. Kosowsky, M. S. Turner, and R. Watkins, Gravitational radiation from colliding vacuum bubbles, Phys. Rev. D **45**, 4514 (1992).
[214] A. Kosowsky, M. S. Turner, and R. Watkins, Gravitational Waves from First Order Cosmological Phase Transitions, Phys. Rev. Lett. **69**, 2026 (1992).
[215] A. Kosowsky and M. S. Turner, Gravitational radiation from colliding vacuum bubbles: Envelope approximation to many bubble collisions, Phys. Rev. D **47**, 4372 (1993).
[216] M. Kamionkowski, A. Kosowsky, and M. S. Turner, Gravitational radiation from first order phase transitions, Phys. Rev. D **49**, 2837 (1994).
[217] C. Caprini, R. Durrer, and G. Servant, Gravitational wave generation from bubble collisions in first-order phase transitions: An analytic approach, Phys. Rev. D **77**, 124015 (2008).
[218] S. J. Huber and T. Konstandin, Gravitational wave production by collisions: More bubbles, J. Cosmol. Astropart. Phys. 09 (2008) 022.
[219] M. Hindmarsh, S. J. Huber, K. Rummukainen, and D. J. Weir, Gravitational Waves from the Sound of a First Order Phase Transition, Phys. Rev. Lett. **112**, 041301 (2014).
[220] J. T. Giblin, Jr. and J. B. Mertens, Vacuum bubbles in the presence of a relativistic fluid, J. High Energy Phys. 12 (2013) 042.
[221] J. T. Giblin and J. B. Mertens, Gravitional radiation from first-order phase transitions in the presence of a fluid, Phys. Rev. D **90**, 023532 (2014).
[222] M. Hindmarsh, S. J. Huber, K. Rummukainen, and D. J. Weir, Numerical simulations of acoustically generated gravitational waves at a first order phase transition, Phys. Rev. D **92**, 123009 (2015).
[223] C. Caprini and R. Durrer, Gravitational waves from stochastic relativistic sources: Primordial turbulence and magnetic fields, Phys. Rev. D **74**, 063521 (2006).
[224] T. Kahniashvili, A. Kosowsky, G. Gogoberidze, and Y. Maravin, Detectability of gravitational waves from phase transitions, Phys. Rev. D **78**, 043003 (2008).
[225] T. Kahniashvili, L. Campanelli, G. Gogoberidze, Y. Maravin, and B. Ratra, Gravitational radiation from primordial helical inverse cascade MHD turbulence, Phys. Rev. D **78**, 123006 (2008); **79**, 109901(E) (2009).
[226] T. Kahniashvili, L. Kisslinger, and T. Stevens, Gravitational radiation generated by magnetic fields in cosmological phase transitions, Phys. Rev. D **81**, 023004 (2010).
[227] L. Kisslinger and T. Kahniashvili, Polarized gravitational waves from cosmological phase transitions, Phys. Rev. D **92**, 043006 (2015).
[228] C. Caprini, R. Durrer, and G. Servant, The stochastic gravitational wave background from turbulence and magnetic fields generated by a first-order phase transition, J. Cosmol. Astropart. Phys. 12 (**2009**) 024.
[229] J. Ellis, M. Lewicki, and J. M. No, On the maximal strength of a first-order electroweak phase transition and its gravitational wave signal, J. Cosmol. Astropart. Phys. 04 (2019) 003.
[230] J. Ellis, M. Lewicki, and J. M. No, Gravitational waves from first-order cosmological phase transitions: Lifetime of the sound wave source, J. Cosmol. Astropart. Phys. 07 (2020) 050.
[231] X. Wang, F. P. Huang, and X. Zhang, Phase transition dynamics and gravitational wave spectra of strong first-order phase transition in supercooled universe, J. Cosmol. Astropart. Phys. 05 (2020) 045.
[232] J. R. Espinosa, T. Konstandin, J. M. No, and G. Servant, Energy budget of cosmological first-order phase transitions, J. Cosmol. Astropart. Phys. 06 (2010) 028.
[233] K. Schmitz, New sensitivity curves for gravitational-wave signals from cosmological phase transitions, J. High Energy Phys. 01 (2021) 097.
[234] D. Bodeker and G. D. Moore, Electroweak bubble wall speed limit, J. Cosmol. Astropart. Phys. 05 (2017) 025.
[235] G. D. Moore and T. Prokopec, How fast can the wall move? A study of the electroweak phase transition dynamics, Phys. Rev. D **52**, 7182 (1995).

[236] A. Megevand and A. D. Sanchez, Velocity of electroweak bubble walls, Nucl. Phys. **B825**, 151 (2010).
[237] S. J. Huber and M. Sopena, An efficient approach to electroweak bubble velocities, arXiv:1302.1044.
[238] T. Konstandin, G. Nardini, and I. Rues, From Boltzmann equations to steady wall velocities, J. Cosmol. Astropart. Phys. 09 (2014) 028.
[239] G. C. Dorsch, S. J. Huber, and T. Konstandin, Bubble wall velocities in the standard model and beyond, J. Cosmol. Astropart. Phys. 12 (2018) 034.
[240] B. Laurent and J. M. Cline, First principles determination of bubble wall velocity, Phys. Rev. D **106**, 023501 (2022).
[241] X. Wang, F. P. Huang, and X. Zhang, Bubble wall velocity beyond leading-log approximation in electroweak phase transition, arXiv:2011.12903.
[242] C. Caprini, M. Hindmarsh, S. Huber, T. Konstandin, J. Kozaczuk, G. Nardini, J. M. No, A. Petiteau, P. Schwaller, G. Servant *et al.*, Science with the space-based interferometer eLISA. II: Gravitational waves from cosmological phase transitions, J. Cosmol. Astropart. Phys. 04 (2016) 001.
[243] C. Caprini, M. Chala, G. C. Dorsch, M. Hindmarsh, S. J. Huber, T. Konstandin, J. Kozaczuk, G. Nardini, J. M. No, K. Rummukainen *et al.*, Detecting gravitational waves from cosmological phase Transitions with LISA: An update, J. Cosmol. Astropart. Phys. 03 (2020) 024.
[244] G. Janssen, G. Hobbs, M. McLaughlin, C. Bassa, A. T. Deller, M. Kramer, K. Lee, C. Mingarelli, P. Rosado, S. Sanidas *et al.*, Gravitational wave astronomy with the SKA, Proc. Sci. AASKA14 (**2015**) 037.
[245] P. Amaro-Seoane *et al.* (LISA Collaboration), Laser interferometer space antenna, arXiv:1702.00786.